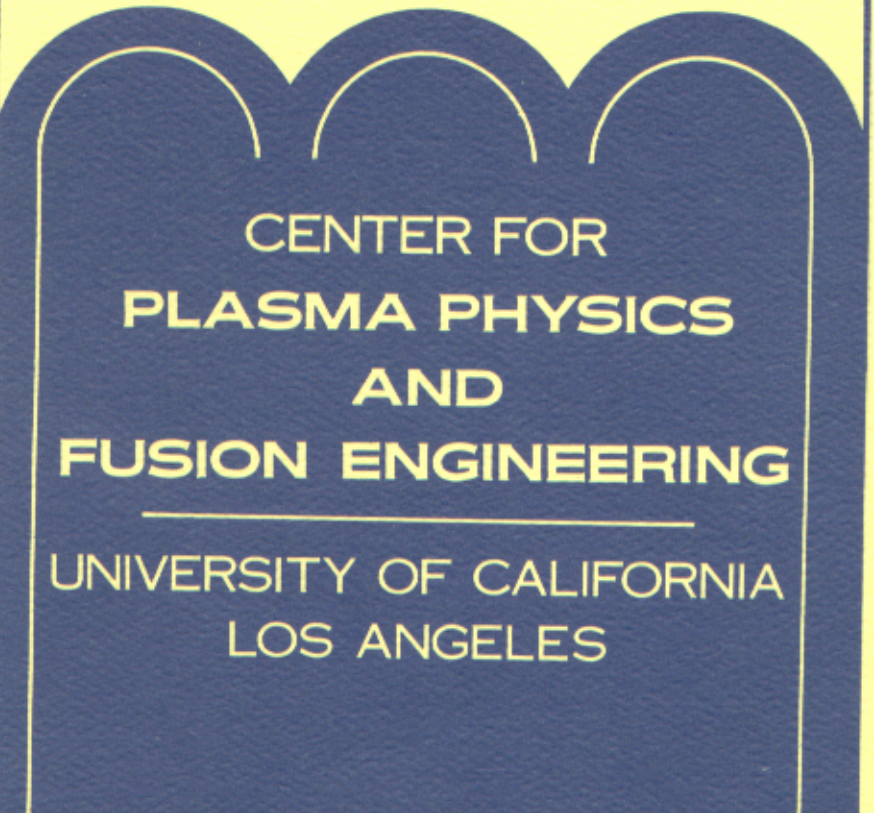


STATUS OF MULTIPOLE-SURMACS
AS CANDIDATES FOR
ADVANCED FUEL FUSION REACTORS

Francis F. Chen

PPG-553

March 1981



CENTER FOR
PLASMA PHYSICS
AND
FUSION ENGINEERING

UNIVERSITY OF CALIFORNIA
LOS ANGELES

STATUS OF MULTIPOLE-SURMACS
AS CANDIDATES FOR
ADVANCED FUEL FUSION REACTORS

Francis F. Chen

PPG-553

March 1981

Electrical Sciences and Engineering Department
University of California, Los Angeles 90024

Presented at the course on Unconventional Approaches to Fusion,
International School of Fusion Reactor Technology,
Erice, Sicily, March 16-25, 1981.

MULTIPOLES AND SURMACS I: PHYSICS

Francis F. Chen

Electrical Sciences and Engineering Department
University of California
Los Angeles, California 90024

GENERAL CONCEPT

The basic idea in surface magnetic field (surmac) devices¹ is to create a magnetic fence surrounding a large volume of reacting plasma (Fig. 1). The field is created by an inner set of conductors, immersed in the plasma, which carry current in the same direction. The return current is carried in an outer set of conductors which lie outside the plasma and need not be inside the vacuum wall. Since the lines of force have alternately good and bad curvature, hydromagnetic instabilities are strongly stabilized by average-minimum-B. The large enclosed volume of field-free plasma cannot emit synchrotron radiation; hence, the major advantage of such devices is purported to be the possibility of burning neutron-free fuels, which require plasma temperatures above 100 keV.

To close the ends of a linear device, one can bend the rods to form a "geometric mirror" (Fig. 2). Though interesting theoretical results for particle confinement for this exist², the leak rate is likely to be much larger than for toroidal configurations. The advantage of externally supported rods, allowing the use of normal conductors, is nullified by the large ohmic dissipation of such rods. A helical set of conductors has also been tried³, producing a toroidal plasma with a minimum of support loss area (Fig. 3). Present experiments are being performed in a simpler version of this, a supported dodecapole⁴ (Fig. 4). The return current is in the walls. For near-term applications⁵ surface fields can be used on an axisymmetric mirror machine⁵ (Fig. 5) to increase the mirror ratio without losing hydromagnetic

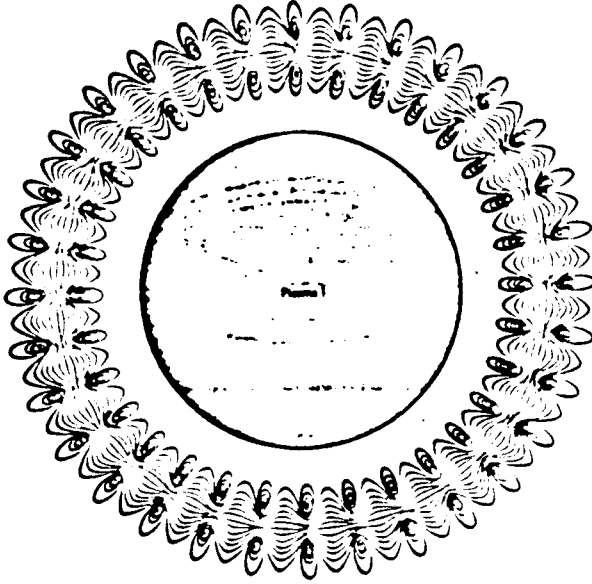


Fig. 1. Idealized surmac field.

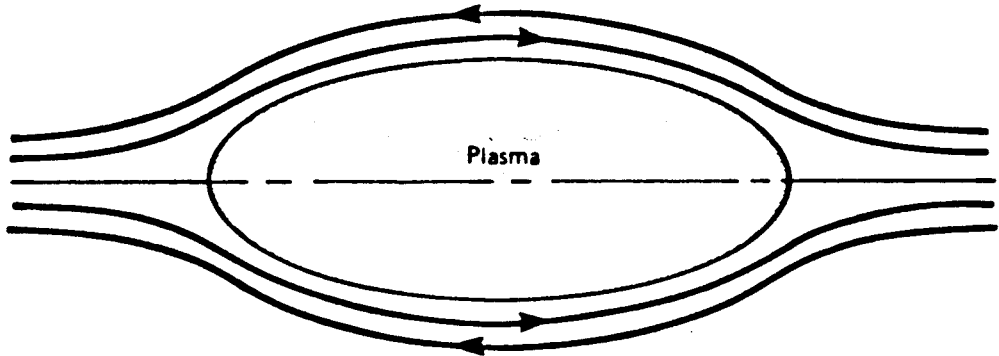


Fig. 2. A linear surmac with geometric mirror.

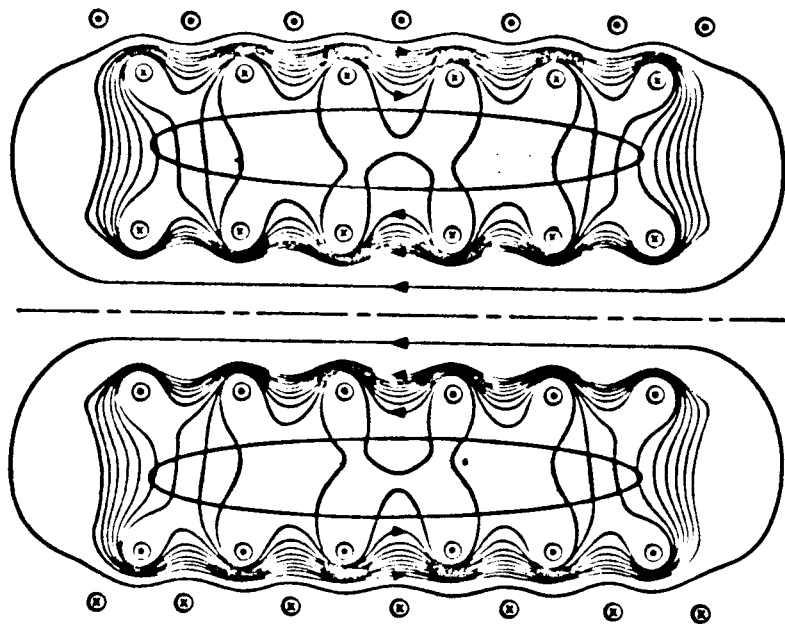


Fig. 3. A triple-helix surmac.

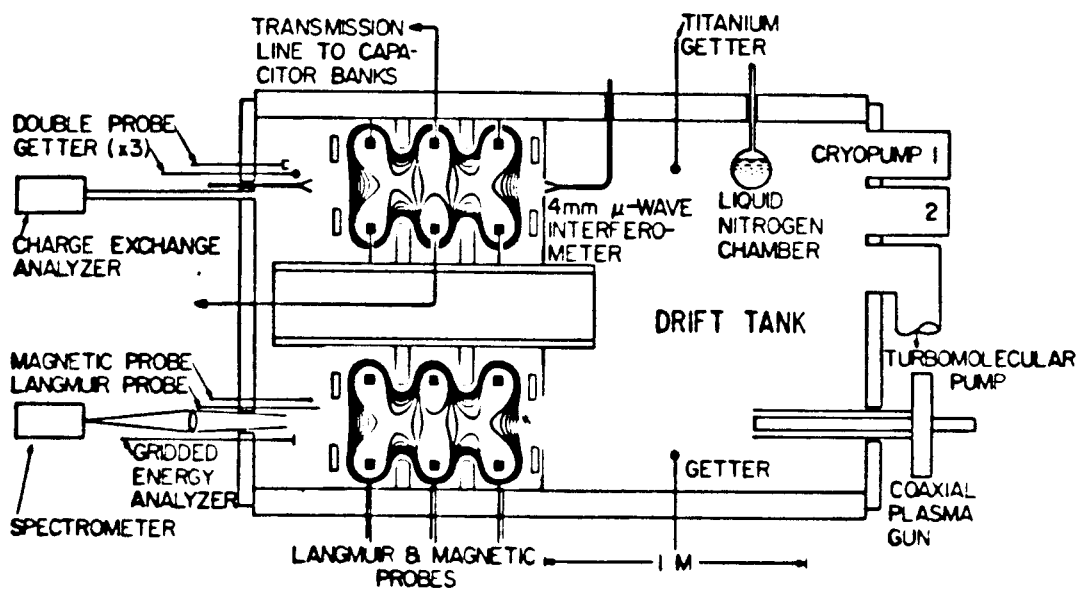


Fig. 4. A toroidal dodecapole with six supported rings.

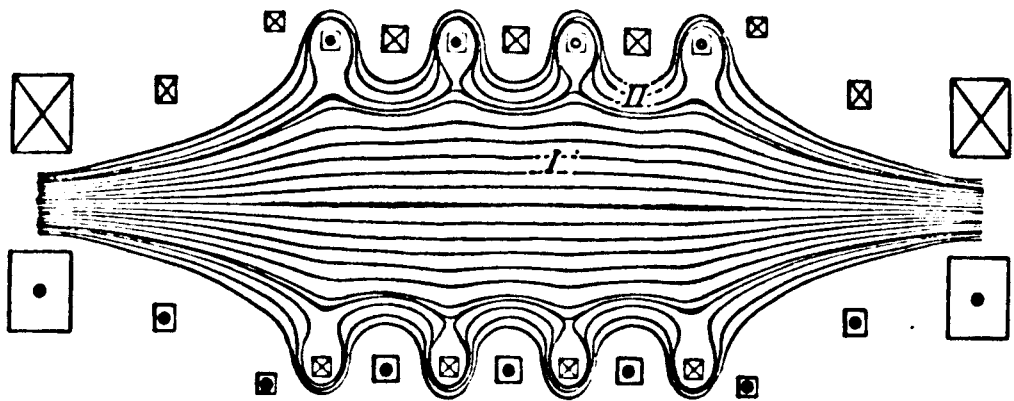


Fig. 5. A surmac-supplemented high-ratio mirror.

stability. By far the most extensively studied configuration, however, is the toroidal octupole⁶ (Fig. 6), containing four supported hoops at General Atomic in La Jolla, California, or four

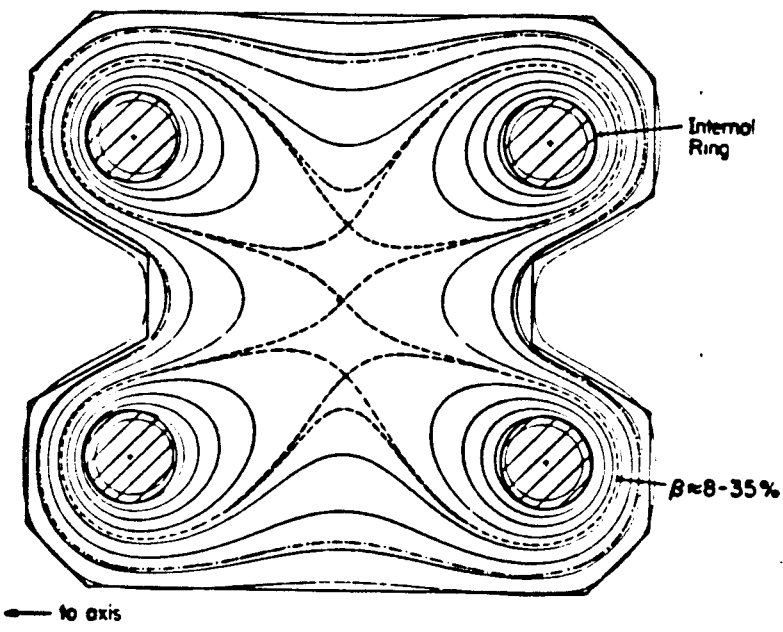


Fig. 6. Cross section of a toroidal octupole. The axis of symmetry is to the left. Return current flows in the walls.

levitated hoops at the University of Wisconsin. We shall use this

as the standard configuration for discussion. Because of the cost of the levitated rings and the plasma losses to them, it is likely that a reasonable reactor design cannot be made with less than four rings or more than six.

MULTIPOLE NOMENCLATURE AND SCALING

The main features of a multipole with poloidal but no toroidal field can be seen in Fig. 6. Near the conductors the field lines encircle only one conductor. This is the region of private flux; there is absolute minimum-B stability here. The dashed lines which cross near the center are separatrices of two types: the minor separatrix connects two rings; the major separatrix connects all the rings. The B-field is zero at the x-type neutral points and is very weak in the region between separatrices. One may assume that the plasma density is uniform and has its maximum value in this region. The region outside the major separatrix is the common flux region, in which the field lines encircle all the conductors. The average curvature is favorable (inward) on the inner flux surfaces but becomes unfavorable (outward) on the outer surfaces. The critical flux surface separating regions of MHD stability and instability, shown by the dot-dash (---) line, is called ψ_{crit} or ψ_c . The plasma density falls to nearly zero at ψ_c , and the wall may be placed anywhere outside this surface. The narrow gap between a conductor and the wall through which plasma particles must circulate is called the bridge region. Since in MHD equilibrium the density is constant along field lines, it has a maximum on the separatrix ψ_s in the bridge region and falls to nearly zero at ψ_c on one side and at the conductor surface on the other. The value of $\beta \equiv 2\mu_0 p/B^2$ is defined differently by various authors, causing some confusion. For p we may take the value of plasma pressure on the separatrix, which should also be the maximum p in the plasma. For B we may take the maximum value on the separatrix in any of the bridge regions.

As particles move adiabatically along field lines, they encounter wildly varying values of $|B|$ but maintain the same flux through their Larmor orbits. For this reason, it is more convenient to solve equations in flux space rather than in coordinate space. For axisymmetric systems this formulation results in simple equations⁷ equivalent to the Grad-Shafranov equation for equilibrium. Here we adopt the approach of Samec⁸ and consider only the simple case of linear multipoles, treating toroidal and other effects as perturbations. When the conductors are straight and all currents flow in the ignorable z direction, the problem becomes two-dimensional, and analytic expressions for the vacuum fields are available. The geometry is shown in Fig. 7. A multipole of order 2N has N conductors arrayed in a circle of radius R about the origin, with each rod carrying a current I. Considering this cross section to be a complex plane $Z = x + iy$, we place

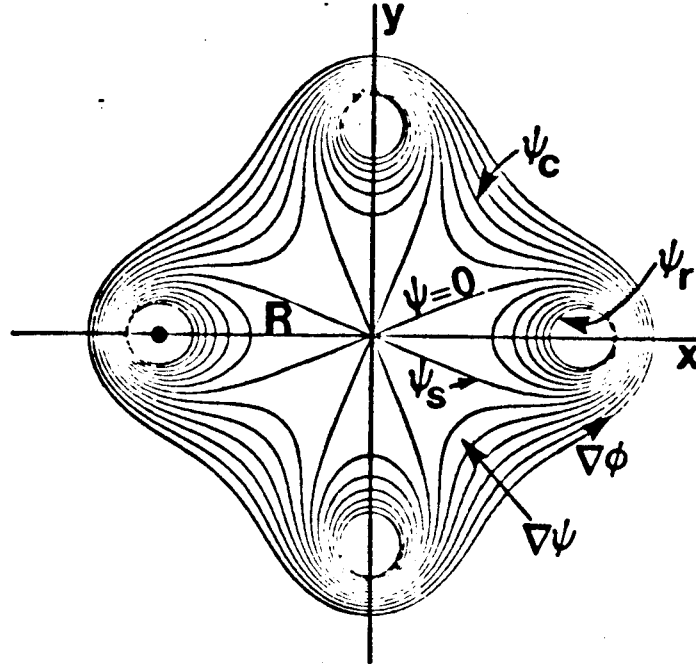


Fig. 7. Coordinate system for linear multipole.

one conductor on the positive x axis. The magnetic flux ψ (per unit length in z) is defined to be 0 on the separatrix ($\psi_s = 0$) and to increase toward the conductor. Thus,

$$\underline{B} = \underline{\nabla}\psi \times \hat{z}, \quad B_x = \partial\psi/\partial y, \quad B_y = -\partial\psi/\partial x. \quad (1)$$

If we define a stream function

$$A = \phi + i\psi, \quad (2)$$

The Cauchy-Riemann conditions give

$$\frac{dA}{dZ} = \frac{\partial\phi}{\partial x} + i \frac{\partial\psi}{\partial x} = \frac{\partial\psi}{\partial y} - i \frac{\partial\phi}{\partial y} = \underline{B} \equiv B_x - iB_y. \quad (3)$$

Thus

$$B_x = \frac{\partial\phi}{\partial x} = \frac{\partial\psi}{\partial y}, \quad B_y = \frac{\partial\phi}{\partial y} = -\frac{\partial\psi}{\partial x}, \quad (4)$$

in agreement with Eq. (1). We also note that $\underline{B} = \underline{\nabla}\phi$, so that ϕ is a coordinate, with dimensions of flux, increasing along \underline{B} . The flux ψ is really the poloidal flux χ in tokamak theory; but since there is no toroidal flux here, there can be no confusion.

We next normalize A to the current I by defining

$$i\phi - \Psi = 2\pi iA/\mu_0 I = (2\pi/\mu_0 I)(i\phi - \Psi). \quad (5)$$

For conductors located at $Z = Re^{2\pi in/N}$, $n = 0, 1 \dots (N-1)$, the flux is given by the simple expression

$$i\phi - \Psi = \ln[(Z/R)^N - 1]. \quad (6)$$

Solving for Z, we obtain an equation for the lines of force:

$$Z = R[1 + \exp(i\phi - \Psi)]^{1/N}, \quad (7)$$

where $\Psi = \text{const.}$ and ϕ goes from 0 to 2π . The magnetic field is found from dA/dZ :

$$\underline{B} = B_x - iB_y = \frac{\mu_0 IN}{2\pi iR} \frac{[1 + \exp(i\phi - \Psi)]^{(N-1)/N}}{\exp(i\phi - \Psi)}. \quad (8)$$

The width of the bridge region can now be found easily. Consider the conductor on the positive x axis ($\phi = 0$). Then Eq. (7) shows that the separatrix ($\Psi = 0$) is located at $x_s = R2^{1/N}$, while the center of the rod ($\Psi = \infty$) is at $x = R$.

The position of Ψ_c is found by evaluating $V' = dV/d\Psi$, where V is the volume of a tube of force. If $ds_1(\ell)$ is the width of a tube of force, we have

$$B = \frac{d\Psi}{ds_1}, \quad dV = \int ds_1(\ell)d\ell, \quad \frac{dV}{d\Psi} = \int d\ell \frac{ds_1}{d\Psi} = \int \frac{d\ell}{B}. \quad (9)$$

Since $\underline{B} = \underline{\nabla}\phi = d\phi/d\ell$, we have from Eqs. (8) and (5)

$$\begin{aligned} V' &= \int \frac{d\phi}{B^2} = \int \frac{d\phi}{BB^*} = \left(\frac{2\pi}{\mu_0 I}\right)^2 \left(\frac{R}{N}\right)^2 \int \frac{e^{-2\Psi} d\phi}{[(1+e^{i\phi-\Psi})(1+e^{-i\phi-\Psi})]^{(N-1)/N}} \\ &= \frac{2\pi R^2}{\mu_0 IN^2} e^{-2\Psi} \int d\phi [1+2e^{-\Psi} \cos\phi + e^{-2\Psi}]^{\frac{1-N}{N}}. \end{aligned} \quad (10)$$

This quantity is easily computed for each line Ψ , resulting in the usual min-B diagram of Fig. 8. Hydromagnetic stability is lost outside the critical surface Ψ_c where this curve has a minimum. The value of Ψ_c , computed from Eq. (10), is well approximated by^{8,9}

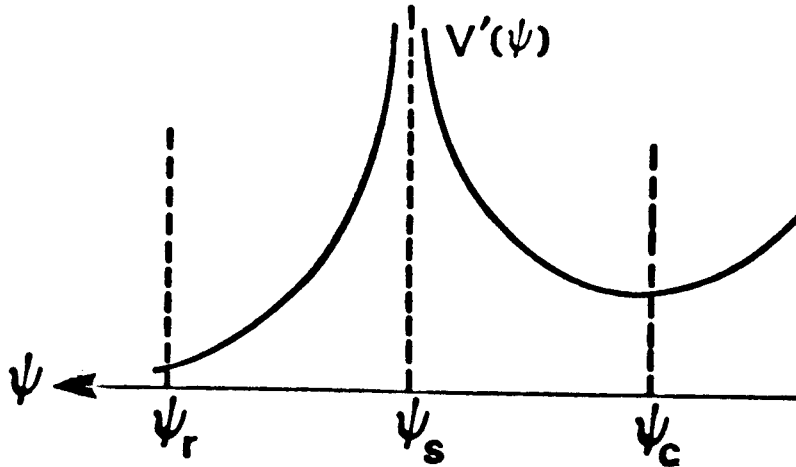


Fig. 8. Qualitative behavior of $V'(\psi) = \int d\ell/B$, the reciprocal of the magnetic well in a multipole.

$$\Psi_c(N) = 0.243 - 0.615 \ln N + 0.0125 (\ln N)^2 < 0. \quad (11)$$

These formulas permit a simple comparison of multipoles of different orders. For each value of N , the rate of plasma transport loss is determined by $-\Psi_c(N)$; this increases with N , as shown in Table I. One usually assumes that the loss rate will not be diminished if the conductor surface is located at least as far away from ψ_s in flux space as ψ_c is; namely, at $\psi_r = -\psi_c$. The width of the bridge region, $d = x_c - x_r$, is found from Eq. (7) for $\phi = 0$:

$$x_r, x_c = R[1 + \exp(\pm \psi_c)]^{1/N}. \quad (12)$$

The radius a of the rod or ring is

$$a = x_r - R = R[(1 + \exp \psi_c)^{1/N} - 1]. \quad (13)$$

We see from Table I that $|\psi_c|$ increases with N , indicating better confinement, even though the width d of the bridge decreases with N (for constant I and R). The quadrupole ($N=2$) is exceptionally bad in this regard. The space available for the conductor, indicated by a/R , decreases monotonically with N . For confinement of the most energetic particles, d must contain a few Larmor radii, say 6. This means that Bd has a minimum value, or, since d/R is given, BR must exceed a certain number. For the 15-MeV protons from the D-He³ reaction, this number is 3.36. The required value of BR (with B given its value at the separatrix)

Table I. Scaling of Linear Multipoles with N Rods

| N = | 2 | 4 | 6 | 8 | 12 |
|---------------------------|-------|-------|-------|-------|-------|
| $-\psi_c$ | 0.177 | 0.586 | 0.819 | 0.982 | 1.208 |
| d/R | 0.125 | 0.176 | 0.155 | 0.136 | 0.108 |
| a/R | 0.356 | 0.117 | 0.063 | 0.041 | 0.022 |
| BR(15MeV H ⁺) | 26.8 | 19.1 | 21.6 | 24.7 | 31.0 |
| I(MA) | 47.3 | 14.2 | 10.1 | 8.4 | 6.9 |
| jR^2 (MA) | 119 | 330 | 810 | 1591 | 4538 |

is seen from Table I to increase with N for $N > 2$. Since superconductors probably cannot produce fields larger than 10T, we see that $R \approx 2$ m is required even for the optimum case of the octupole ($N=4$). From Eq. (8) one sees that $BR = I \times f(N)$ for $\phi = \psi = 0$; hence, the required current I is independent of R. It decreases monotonically with N and is of reasonable magnitude. The current density j, however, increases sharply with N because \underline{a} decreases. The value of jR^2 shown in Table I indicates that high-order multipoles are impractical. An unshielded superconductor can carry perhaps 30 MA/m², requiring $R = 3.3$ m for the octupole and $R = 5.2$ m for the dodecapole ($N=6$). A shielded conductor with 1 m of neutron and x-ray shielding can have a net current density of only 3 MA/m², requiring $R=10$ and 16 m, respectively. These estimates will be seen to be somewhat conservative. Increasing N improves the β limit as well as the confinement time. The engineering limits on current density and machine size, however, will probably cause the optimal conditions to occur for $4 \leq N \leq 6$.

HYDROMAGNETIC STABILITY

The basic minimum- \bar{B} principle that the plasma is stable inside ψ_c applies only to flute modes, whose amplitude is constant along \underline{B} . One must also guard against ballooning modes, which are localized in the regions of bad curvature and therefore do not sample the stabilizing effect of the good curvature regions. The standard method for treating this problem is the energy principle of Bernstein et al.¹⁰, in a form applicable to axisymmetric toruses with no toroidal field^{11,12}. Original estimates¹³ of the β limit for ballooning were based on the growth rates of these modes compared with the time for communication at the Alfvén speed between good and bad curvature regions. These estimates

yielded optimistic β 's of the order of 25%. This problem has now been treated more exactly by solving the Euler-Lagrange equation for the shape of the perturbation that minimizes δW . The results^{7,9,13} indicate that the most unstable ballooning modes are not line-tied in the good curvature regions; rather, they are flutelike near ψ_c and become localized only near ψ_s . Since these perturbations require less change in magnetic energy, the β limits are considerably lower, around 4-8%. In addition, the effect of finite β on the equilibrium configuration has been calculated^{7,13} by solving the Grad-Shafranov equation; the β limit is not greatly affected.

Though the details of the stability calculations cannot be given here, the nature of the results can be seen from the example of the linear multipole⁹. For flute modes the instability criterion $\delta W < 0$ can be written⁹

$$(V'' - \mu_0 p' M) [V'' + (p' V' / \gamma p)] < 0, \quad (14)$$

where $p' = dp/d\psi$, $V'' = d^2V/d\psi^2$, $M = \int d\ell/B^3$, and γ is the ratio of specific heats. For $p, p' \rightarrow 0$, the leading term gives $V'' p' V' / \gamma p < 0$, or since γ, p , and $V' = \int d\ell/B$ are positive,

$$V'' p' < 0. \quad (15)$$

This leads to the definition of ψ_c on Fig. 8. When p is finite, the magnetic well can support a finite pressure gradient. In the region between ψ_s and ψ_c , where $V'' > 0$, the second factor in Eq. (14) is positive for $p' > 0$ (the normal direction for p'), and the first factor then is negative if

$$p' > V'' / \mu_0 M. \quad (16)$$

For a reverse gradient, $p' < 0$, the second factor of Eq. (14) is negative if

$$p' < -\gamma p V'' / \mu_0 V' < 0. \quad (17)$$

A stable reverse gradient is possible because of finite plasma compressibility. These limits on p' in the normal and reverse directions also apply to the private flux region, where $V'' < 0$. The value of p' vanishes at the critical layer $V'' = 0$. The value of β on the separatrix is found by integrating Eq. (16) from ψ_c to 0, using the vacuum field shape, and dividing by the known value of B^2 at $\psi = 0$. The result is shown as β_f in Table II.

For ballooning modes at marginal stability ($\delta W = 0$), the displacement X in the $\nabla\psi$ direction must satisfy the Euler equation⁹

$$\frac{\partial}{\partial \phi} \left(\frac{1}{\mu_0 B^2 J} \frac{\partial X}{\partial \phi} \right) - p' D J X(\psi, \phi) = 0, \quad (18)$$

where $D = (-2\mu_0/B^2)(\partial/\partial\psi)(p + B^2/2\mu_0)$ and J is the Jacobian for the transformation from (x, y, z) to (ψ, ϕ, z) . The numerical solutions have the shape described previously. Knowing these functions $X(\psi, \phi)$, one can compute the maximum p' for stability, and then integrate to find the critical β for ballooning. This is shown as β_b in Table II. Except for the quadrupole, flute interchange is more dangerous than ballooning.

Table II. Beta Limits for Low- β Flute and Ballooning Modes⁹

| N = | 2 | 4 | 6 | 12 |
|---------------|-----|------|------|------|
| β_f (%) | 4.7 | 7.3 | 8.9 | 11.7 |
| β_b (%) | 2.7 | 11.0 | 18.0 | 31.0 |

These values of β are large enough to affect the vacuum fields. Now one must assume a pressure profile $p(\psi)$, compute the field shape and the critical $\beta'(\psi)$ it permits, and iterate to find the maximum stable β . It is reasonable to take $p(\psi_c) = p(\psi_r) = 0$ and $p'(\psi_s) = 0$, with $p = p_0 = \text{const.}$ between separatrices if there are more than one. For linear multipoles, Samec⁸ assumes a symmetric profile

$$p(\psi) = p_0 (1 - \psi^2/\psi_0^2), \quad (19)$$

with adjustable parameters p_0 and ψ_0 . For toroidal multipoles, D'Ippolito et al.⁷ take profiles of the form

$$p(\psi) = p_0 \sin^2 \left[\frac{\pi}{2} \left(\frac{\psi - \psi_c}{\psi_{s1} - \psi_c} \right) \right] \quad \text{and} \quad p(\psi) = p_0 \sin^2 \left[\frac{\pi}{2} \left(\frac{\psi - \psi_{s2}}{\psi_r - \psi_{s2}} \right) \right] \quad (20)$$

for the common and private flux regions, respectively. For linear multipoles, where $\underline{B} = \nabla\psi \times \hat{z}$ and $\nabla \times \underline{B} = \mu_0 j \hat{z}$, the force balance equation $\nabla p = \underline{j} \times \underline{B}$ reduces to

$$\nabla^2 \psi + \mu_0 dp/d\psi = 0. \quad (21)$$

With Eq. (19), this becomes

$$\nabla^2 \psi - k^2 \psi = 0, \quad k^2 \equiv 2\mu_0 p_0 / \psi_0^2, \quad (22)$$

with a solution

$$\psi = -\frac{\mu_0 I}{2\pi} \left[\sum_{j=0}^{N-1} \frac{K_0(kR)}{I_0(kR)} I_0(k\rho_j) - K_0(k\rho_j) \right], \quad (23)$$

where ρ_j is the distance to the j^{th} rod. This finite- β equilibrium is then used to compute the critical $p'(\psi)$ or $\beta'(\psi)$ on each surface. A typical result is shown in Fig. 9. Here it is seen that the

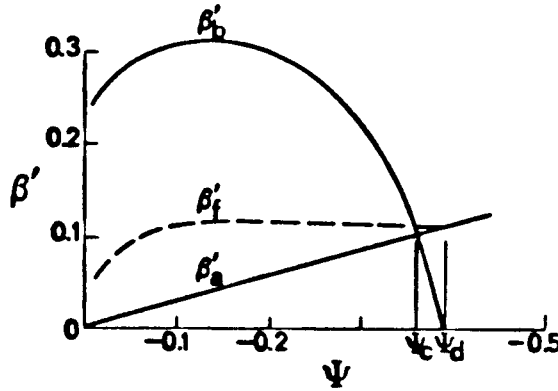


Fig. 9. Profile of flute and ballooning $\beta'(\psi)$ limits for an octupole with $k = 3$ (from Ref. 9).

assumed parabolic $p(\psi)$ gives a linear $\beta'_a(\beta)$ which lies well below the flute and ballooning limits β'_f and β'_b except at the edge. Beyond the surface ψ_c this profile is ballooning unstable; and beyond ψ_d , the surface where the average curvature is zero, the profile is flute unstable. It is clear from Fig. 9 that the parabolic profile does not make optimum use of the stabilization available: integration of β' yields $\beta_a = 1.8\%$, $\beta_f = 4\%$, and $\beta_b = 10\%$. A $p(\psi)$ profile with decreasing rather than increasing slope would give higher β limits, but it may not be consistent with the diffusion mechanism, as we shall see. Theoretical β limits for linear and toroidal multipoles with finite pressure are shown in Table III.

The main effect of finite β on the equilibrium is to push out the field lines where B is weak--in the inward curving regions. Since this diminishes the amount of good curvature, the value of ψ_c goes down. The shape of the field in the bridge region hardly changes, but the stable region gets narrower. This is also seen in Fig. 9: if p_0 is increased, β'_a increases, and ψ_c moves in. It can be shown⁷ that the decrease in ψ_c accounts for almost the entire finite- β effect. Toroidal multipoles have higher β limits than linear multipoles, but only because the β 's are calculated at the outer rings. Unless extraordinary shaping is done, the

Table III. Theoretical β Limits for Finite- β Multipoles (%)

| N = | 2 | 4 | 6 | 12 |
|------------------------|------|-----|-----|-----|
| Linear ⁹ | 0.22 | 1.8 | 3.5 | 8.0 |
| Toroidal ⁷ | 1 | 4 | 7 | - |
| Toroidal ¹³ | - | 3.9 | - | - |

field will be stronger at the inner rings. More magnetic energy is required to perturb the plasma at the inner rings, and therefore flute modes tend to be stabilized by toroidal effects. However, the β values are not larger than for linear multipoles if normalized to the B value at the inner rings.

Whether or not these calculations can be extrapolated to the reactor regime depends on their agreement with observations in present-day plasmas. Unfortunately, the experimental situation is unclear. Recent measurements on the Wisconsin octupole¹⁴ (Fig. 6) showed bridge $\beta = 8\%$, twice the theoretical limit, under the following conditions: $n = 5 \times 10^{13} \text{ cm}^{-3}$, $T_e \approx T_i \approx 15 \text{ eV}$, $B = 860 \text{ G}$, $L_p \approx 5 \rho_i$, $\tau = 600 \text{ } \mu\text{sec}$, where $L_p = p/\nabla p$, ρ_i is the ion Larmor radius, and τ is the decay time. The plasma is created by gun injection; quiescence is reached in $40 \text{ } \mu\text{sec}$. At lower B, a β of 35% was observed with $n = 2 \times 10^{13} \text{ cm}^{-3}$, $T_e \approx T_i \approx 9 \text{ eV}$, $B = 200 \text{ G}$, $L_p = 2 \rho_i$, and $\tau = 350 \text{ } \mu\text{sec}$. In neither case are oscillations observed; beta was limited only by the plasma sources, not by MHD instability. The observation of β 's exceeding the MHD limit was attributed to collisional ion viscosity. Collisionless finite Larmor radius (FLR) effects were claimed to be unimportant because the measured diamagnetic current profiles agreed with both the fluid and FLR predictions. However, this statement applies only to the finite- β equilibrium; the effect of FLR on stability was not treated and could have been the dominant effect.

Recent work on the UCLA dodecapole⁴ (Fig. 4) with gun injection has yielded $\beta = 8\%$ on the outer bridge under conditions where $n = 5 \times 10^{13} \text{ cm}^{-3}$, $T_i = 200 \text{ eV}$, $T_e = 25 \text{ eV}$, $B = 2.3 \text{ kG}$, $\tau_p \approx 2 \text{ ms}$, $\tau_e \approx 100 \text{ } \mu\text{sec}$, and $L_p \approx \rho_i$. Though the theoretical limit for this case⁷ (Table III) is also $\beta \approx 8\%$, the agreement is accidental. The limit on β is imposed by the requirement that the bridge region contain at least one or two Larmor radii; this implies $T_i \propto B^2$, which is observed. The density profile was seen to narrow to half-width $\approx \rho_i$ as β was increased, in agreement with the theoretical picture of finite- β equilibria. No MHD

activity was observed, but a 100 kHz oscillation localized to the bad curvature regions and resembling a drift-ballooning mode was seen for $\beta > 3\%$, when the density profile has steepened. Since the conditions here are more collisionless than in the Wisconsin experiment, collisionless FLR effects probably cause stabilization of MHD modes. The B field is being increased to 6 kG to increase L_p/ρ_i ; but if neutral-beam heating is also used to increase T_i to the $L_p = \rho_i$ limit, the MHD ballooning theory will remain untested.

We now discuss possible ways to increase the rather low predicted β limits. 1) Toroidal effects, as we have seen, can increase the β on the outer hoops, but not the overall β . 2) Wall stabilization can help, but the calculations of Ref. 13 already incorporated this effect. 3) The use of square rather than circular arrays (Fig. 4) may affect β , but the work of Ref. 7 treated square arrays without yielding a significantly different value of β . 4) The calculations reported here assumed infinitely short wavelength in the z (toroidal) direction. This permitted each ψ surface to be analyzed separately. A recent calculation¹⁵ for finite toroidal m-no. reveals that β can be doubled if $m > 20$ modes are suppressed. 5) FLR stabilization is a strong effect which apparently dominates the experiments. So far no theory of finite- ρ_i MHD modes in multipoles exists. In a reactor, there will always be a number of large-orbit reaction products, and these could play an important role in short-circuiting potential fluctuations. 6) Another important effect is that of shear. If a toroidal field is added, it will increase synchrotron radiation, but, as we shall see, perhaps not significantly, since the surface region dominates the synchrotron losses. Theoretical estimates of β in a sheared system exist only for single-ring levitrons; indications are that much larger β 's can be attained. Thus, the two best hopes for larger β , effects (5) and (6), are not yet analyzed theoretically.

CROSS-FIELD TRANSPORT

In the last 15 years research on multipoles, spherators, and levitrons have yielded a large amount of information on classical and anomalous transport mechanisms. This large body of work has recently been summarized in table form⁹ and discussed critically¹⁶. Losses can be caused by field errors, guarded or unguarded ring supports, or convective cells connected with supports. We dispense with field errors as a known phenomenon that can be suppressed by proper design. Guarded supports will be treated later. The main loss mechanisms are 1) classical diffusion, 2) anomalous diffusion with Bohm scaling, and 3) vortex diffusion. Most results come from the GA and UW octupoles.

First we consider the results with poloidal field only. In collisional plasmas such that $v_{ei} \leq v_e/L_c$, where v_e is the electron thermal speed and L_c the connection length between good and bad curvature regions, classical diffusion is observed¹⁷ with $D = D_c \propto n/B^2 T_e^{1/2}$. Furthermore, in almost all experiments the plasma is quiescent inside ψ_c and noisy outside ψ_c . Thus, the effectiveness of min- \bar{B} stabilization at low β seems well established. At lower density, Bohm scaling ($D_B = KT_e/16eB$) is observed¹⁸, but with a much smaller coefficient: $D = D_B/300$. At high B and low n , the GA group observed¹⁹ that \sqrt{n} decayed linearly with time, implying $D \propto n^{-1/2}$; more precisely, $D \propto (T/Mn)^{1/2}$. This is exactly the dependence predicted by Okuda and Dawson²⁰ for convective transport in thermal-level vortex motions. The coefficient was also about right, so $D \approx 3 D_{OD}$, and was not affected by weak shear. Note that D_{OD} is independent of B .

The UW octupole experiments at Wisconsin were dominated by vortex diffusion²¹ at a hyperthermal level: $D = 30 D_{OD} \propto n^{-1/2}$. The dc convective cell patterns could be mapped out with probes²². Since D_{OD} scales as $(T/\epsilon)^{1/2} B^{-1}$, where ϵ is the low frequency dielectric constant $\epsilon = 1 + \Omega_p^2/\Omega_c^2 = 1 + c^2/v_A^2$, expects that vortex diffusion would change from $D_{OD} \propto (T/n)^{1/2}$ to $D_{OD} \propto T^{1/2}/B$ as ϵ approaches 1. This change in scaling has been observed²³. It is now believed¹⁶ that the strong convective patterns are produced by the plasma gun injecting the plasma; the pulsed nature of the levitated rings did not permit waiting until the cells decayed to thermal level, as could be done on the dc octopole at GA. Enhanced vortex diffusion could be reduced to classical diffusion by viscous damping²⁴ or by shear²⁴. The addition of 100 G of toroidal B-field reduced D by a factor of 20.²⁵ In all these experiments the oscillations could not account for the losses, contributing at most $D = D_B/1000$.

When shear is added with a toroidal field, an additional stabilization mechanism is active; furthermore, the field lines are no longer closed, and potentials between field lines can be shorted out. The tokamak regimes of banana, plateau, and Pfirsch-Schluter diffusion were first seen in the GA octopole²⁶. Vortex diffusion is also greatly reduced. Early UW experiments²⁷ showed a large reduction in fluctuation level with shear, but no overall change in confinement. Measurements at GA in the trapped electron regime²⁸ indicated a poloidal Bohm diffusion rate, where $D = D_{BP}/1000$, D_{BP} being D_B evaluated with the poloidal field only. Though experiments on other machines such as tokamaks also could be fitted to this law, the fit is probably accidental, since the Alcator results contradict this. Recent work at UW²⁹ revealed vortex diffusion in the private flux region and two collisionless trapped ion modes in the common flux region; these increased diffusion by an order of magnitude. At GA²⁹, a 40% amplitude

trapped electron mode was observed, peaking near ψ_c , as well as a 20% amplitude ion mode inside ψ_s .

To summarize, it appears that, with poloidal field alone, a gentle plasma production mechanism may allow D to be as small as D_c or D_{OD} , which would be small enough for reactor purposes. With a toroidal field added, D_{OD} should be even smaller, but microinstabilities are found to arise, possibly leading to D's scaling as $10^{-3} D_B$. The ultimate relevance of these modes is not yet known.

To estimate the value of $n\tau$ for any given diffusion coefficient D, one must solve the diffusion equation

$$\frac{\partial n}{\partial t} = \nabla \cdot (D \nabla n). \quad (24)$$

Again, we may use Samec's⁹ two-dimensional example of linear multipoles for illustration. If we further assume n to be constant along field lines, $n = n(\psi, t)$, the problem becomes one-dimensional. Then we have from Eq. (9) $\nabla n = \nabla_{\perp} n = dn/ds_{\perp} = B dn/d\psi$. Eq. (24) becomes

$$\frac{\partial n}{\partial t} = B \frac{\partial}{\partial \psi} \left(DB \frac{\partial n}{\partial \psi} \right), \quad \frac{1}{B} \frac{\partial n}{\partial t} = \frac{\partial}{\partial \psi} \left(DB \frac{\partial n}{\partial \psi} \right). \quad (25)$$

Integrating over $d\ell$ and defining

$$\bar{D} = \int DB d\ell, \quad V' = \int d\ell/B, \quad (26)$$

we obtain

$$\frac{\partial n}{\partial t} = \frac{1}{V'} \frac{\partial}{\partial \psi} \left(\bar{D} \frac{\partial n}{\partial \psi} \right), \quad (27)$$

with V' given by Eq. (10). The solution $n(\psi, t)$ will depend on the form of D. For constant temperature, the three possible diffusion laws described above give

$$\text{classical:} \quad D_c = \alpha_c n/B^2, \quad \bar{D} = \alpha_c n V' \quad (28)$$

$$\text{Bohm:} \quad D_B = \alpha_B/B, \quad \bar{D} = \alpha_B L \quad (29)$$

$$\text{Okuda-Dawson:} \quad D_{OD} = \alpha_D (nL)^{-1/2}, \quad \bar{D} = \alpha_D \mu_0 I' (nL)^{-1/2} \quad (30)$$

where $L = \int d\ell$ and we have used Eq. (26). In Eq. (30), $\int B d\ell$ has been replaced by $\mu_0 I'$, where I' is the sum of all currents

enclosed by the field line. $L(\Psi)$ is found by integrating Eq. (7) over ϕ .

The nature of the problem can be illustrated by taking the case of classical diffusion. Eqs. (27) and (28) then give

$$V' \frac{\partial n}{\partial t} = \alpha_c (nV'n')', \quad ' = \partial/\partial\psi. \quad (31)$$

Separating variables, we let

$$n(\xi, t) = n_0 S^{\frac{1}{2}}(\xi) T(t), \quad (32)$$

where

$$T = (1 + t/\tau_c)^{-1} \text{ and } \xi = \psi/|\psi_c|. \quad (33)$$

Straightforward substitution then yields the spatial equation

$$\frac{d^2 S}{d\xi^2} + \frac{d}{d\xi} (\ln V') \frac{dS}{d\xi} + \lambda \sqrt{S} = 0, \quad (34)$$

where

$$\lambda = 2\psi_c^2/n_0\alpha_c\tau_c \quad (35)$$

The boundary conditions are

$$\begin{aligned} n(\psi_c) = 0 & \quad \text{or} \quad S(-1) = 0 \\ n'(\psi_s) = 0 & \quad \text{or} \quad S'(0) = 0 \\ n(\psi_r) = 0 & \quad \text{or} \quad S(1) = 0 \end{aligned} \quad (36)$$

If we require in addition $S(0^+) = S(0^-)$, the interior and exterior solutions would give different values of τ_c . For the same τ_c , $S(0^+)$ would be larger than $S(0^-)$ because classical diffusion is slower toward and rods than toward ψ_c , owing to geometrical effects. In practice, the matching of solutions at the separatrix may be affected by convection between separatrices. A reasonable approach would be to solve for the exterior region and match at $\xi = 0$ to an interior solution with the same τ_c . Then n would fall to 0 before the surface $\psi = -\psi_c$, allowing us more space for the conductor than previously assumed.

The numerical solution of Eq. (34) is delicate because $S' \rightarrow \infty$ at $\psi = \psi_c$. The density profiles⁹ resemble parabolas, with n falling to 0 much closer to ψ_s as N is increased. To see the scaling of τ_c with N , we can use an approximation good to 20%:

$$\tau_c^* = \delta^2/D = \delta^2 B_o^2 / \alpha_c n_o , \quad (37)$$

where $\delta = x(\psi_c) - x(0)$ is found from Eqs. (7) and (11). Then τ_c^* can be written

$$\tau_c^* = (\psi_c^2 / \alpha_c n_o) T_c^* , \quad T_c^*(N) = (\delta/R)^2 (2N/2^{1/N} \psi_c)^2 . \quad (38)$$

Here α_c is the Spitzer coefficient, and the $B^2 \delta^2 / n_o$ dependence of classical diffusion is evident. The values of T_c^* and of the exact value T_c are shown in Table IV. There is a slow increase of confinement time with multipole order; the rapid increase³⁰ found with assumed trapezoidal profiles of $n(\psi)$ does not hold true. Note that classical diffusion would give $n'(\psi)$ increasing outwards, just opposite in shape to profiles which would give the highest β limit.

Table IV. Scaling of Diffusion Times with Multipole Order⁹

| N = | | 2 | 4 | 6 | 8 | 12 |
|--------------|----------|------|------|------|------|------|
| Classical | T_c | 1.42 | 1.67 | 1.78 | 1.84 | 1.89 |
| (approx.) | T_c^* | 1.14 | 1.42 | 1.56 | 1.65 | 1.76 |
| Bohm | T_B | 0.18 | 0.49 | 0.56 | 0.56 | 0.51 |
| (approx.) | T_B^* | 0.23 | 0.39 | 0.38 | 0.35 | 0.29 |
| Okuda-Dawson | τ_D | 0.25 | 2.27 | 2.40 | 2.26 | 1.68 |

For Bohm scaling, the decay is exponential in time, and we can factor $n(\psi, t)$ into

$$n(\psi, t) = G(\psi) \exp(-t/\tau_B) . \quad (39)$$

Eqs. (27) and (29) then give

$$\frac{d^2 G}{d\xi^2} + \frac{d}{d\xi} (\ln L) + \lambda \frac{v'}{L} G(\xi) = 0 , \quad (40)$$

with $\lambda = \psi_c^2 / \alpha_B \tau_B$ and $G(-1) = G'(0) = 0$. Numerical solution of Eq. (40) leads to density profiles which resemble triangles and are not sensitive to N . The eigenvalue λ leads to a Bohm time T_B given by

$$\tau_B = (\psi_c R / \alpha_B \pi) T_B , \quad (41)$$

and an estimate T_B^* can be made by taking $\tau_B^* = \delta^2/D_B$. These are shown in Table IV. Note that T_B has a maximum around $N = 7$.

Finally, Okuda-Dawson scaling leads to the factorization

$$n(\psi, t) = n_0 (1 - \tau/\tau_D)^2 F^2(\xi) \quad (42)$$

and the eigenvalue

$$\frac{d^2 F}{d\xi^2} - \frac{1}{2} \frac{d}{d\xi} (\ln \hat{L}) \frac{dF}{d\xi} + \hat{\lambda} \hat{V}' \hat{L}^{1/2} F^2(\xi) = 0, \quad (43)$$

where

$$\lambda = \psi_c^2 n_0^{1/2} / \alpha_D \tau_D \nu_0 I \quad \text{and} \quad \hat{\lambda} = R^{5/2} \psi_c^2 n_0^{1/2} / \pi^{1/2} \alpha_D \tau_D. \quad (44)$$

The dependence of τ_D on $n^{1/2}$ is seen here. Since D_{OD} is independent of B , the quantities λ , L , and V' have been normalized to fixed B and R , as shown in Eq. (44). The numerical solution⁹ of Eq. (43) results in a peaked $n(\psi)$ profile somewhat more triangular than a Gaussian. These profiles should be a better fit to the local β limit than the classical profiles. The relative values of $\tau_D(N)$ shown in Table IV indicate a peak at $N = 6$.

In summary, once the transport scaling law is known, the confinement time can be calculated easily for the vacuum field of linear multipoles. It appears that $N = 6$ is near the optimum regardless of the scaling law. Classical diffusion gives asymmetric profiles in ψ space which leave more room for the conductor than normally available. It is also possible, of course, that different scaling laws could be operative in different regions of ψ space.

SYNCHROTRON RADIATION

The reduction of synchrotron radiation by surface confinement is critical to the use of advanced fuels; yet an accurate evaluation of this effect, because of its difficulty, is only now being conducted. Initial optimism was based on the large value of $\langle \beta \rangle$, where the averaging includes the large volume of almost field-free plasma. Single-particle radiation, however, varies as

$$P_s = 5 \times 10^{-26} n_e^2 T_{\text{keV}}^2 \beta^{-1} W/m^3, \quad (45)$$

so that one should average β^{-1} instead of β ; the low- β bridge region then dominates. To be more specific, let us compare two cylindrical plasmas with the same n , T , and volume, one (A) with magnetic field in a shell of radius R and thickness $d \ll R$, and the other (B) with field everywhere (Fig. 10).

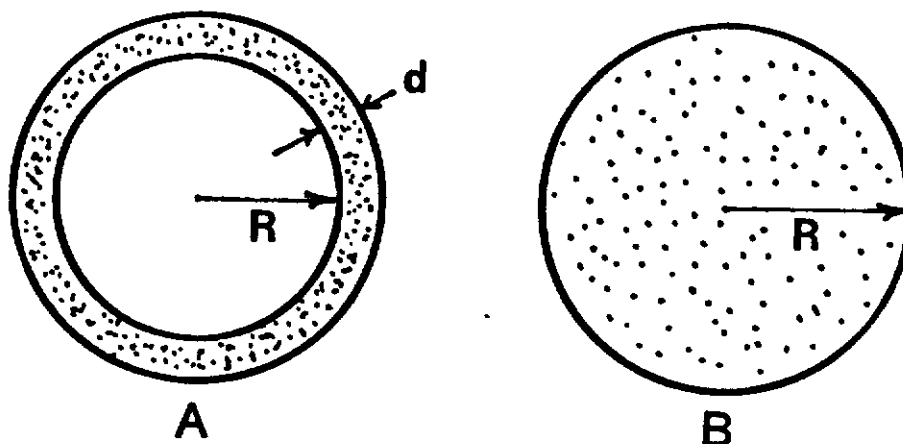


Fig. 10. Comparison of surmac (A) and tokamak (B) for synchrotron radiation.

We neglect reabsorption for the time being. Let us require that the particle confinement τ be equal for these two cases. For classical diffusion, $D = \alpha_c n / B^2$, and the radial flux Γ is given by $\Gamma = 2\pi R j$, where

$$\begin{aligned}
 j &= -D\nabla n = \alpha_c n^2 / B_A^2 d \text{ in (A), and} \\
 &= 2\alpha_c n^2 / B_B^2 R \text{ in (B) .}
 \end{aligned}
 \tag{46}$$

Thus the confinement times $\tau = N / (dN/dt) = N / \Gamma$ are

$$\begin{aligned}
 \tau_A &= \frac{\pi R^2 n}{2\pi R} \frac{B_A^2 d}{\alpha_c n^2} = \frac{R d B_A^2}{2n\alpha_c} \\
 \tau_B &= \frac{\pi R^2 n}{2\pi R} \frac{B_B^2 R}{2\alpha_c n^2} = \frac{R^2 B_B^2}{4n\alpha_c} .
 \end{aligned}
 \tag{47}$$

For these to be equal we must have

$$B_A / B_B = (R/2d)^{1/2} .
 \tag{48}$$

The synchrotron radiation, from Eq. (45), is

$$W_A = C 2\pi R d B_A^2, \quad W_B = C \pi R^2 B_B^2. \quad (49)$$

Eq. (48) then requires $W_A/W_B = 1$. The radiation is not reduced at all if B is increased in a multipole-surmac to keep the diffusion losses the same. The only advantage of a surmac lies in the better filling factor, which gives a higher fusion power. If Bohm diffusion is assumed, the situation is even worse: one obtains $W_A/W_B = R^3/2d^3 \gg 1$. Okuda-Dawson scaling is independent of B. In this case the loss rates are equal only if $R/d = \sqrt{2}$, in which case $W_A/W_B = \sqrt{2}$.

In large plasmas the lower harmonics of the cyclotron frequency are reabsorbed before they escape, and the synchrotron losses are not as large as in Eq. (45). For harmonics lower than a critical harmonic m^* , the plasma radiates like a black body from its surface; higher harmonics have lower amplitude but are not reabsorbed. An early estimate by Dawson³¹ for a p-B¹¹ reactor with $T_i = 2T_e = 300$ keV showed that $m^* = 13$ would be required for synchrotron radiation to be lower than bremsstrahlung, and that this was possible if $\beta = 1$ and walls of reflectivity $r = 97\%$ were used. Since $\beta = 1$ is apparently not achievable because of ballooning, more accurate estimates need to be made. Theoretical results exist only for simple slabs of thickness L. For instance, Trubnikov³² gives, in simplified form⁹:

$$I_s = 0.08(1-r)T_{\text{keV}} B^3 m^{*3} \text{ W/m}^2, \quad m^{*3} = 12.5T_{\text{keV}} \left(\frac{\beta_e BL}{1-r} \right)^{1/2}. \quad (50)$$

In the limit of large reabsorption, we see that W scales as the surface area times $B^{5/2}$. In the example of Fig. 10, both (A) and (B) have the same surface area; hence, from Eq. (48), we have

$$W_A/W_B = (B_A/B_B)^{5/2} = (R/2d)^{5/4} > 1. \quad (51)$$

Again, we find that surface fields do not offer an obvious gain.

In practice, reactor designs are likely to be limited not so much by classical diffusion as by the maximum field achievable with superconductors. In Fig. 10, if (A) and (B) have the same B_{max} and β_{max} , so that n is the same, then W_A/W_B is the ratio of magnetic volumes $2d/R$ if there is no reabsorption, and is the ratio of areas (=1) if there is complete reabsorption. Surface fields have a gain which lies in between, but only at the expense of T_c , which scales as $2d/R$.

To investigate the dependence on N, Samec⁹ has evaluated \bar{P}_s averaged over the linear multipole fields given by Eq. (8). He finds that \bar{P}_s is constant to within $\pm 11\%$ for $3 \leq N \leq 10$. To estimate $n\tau$, he approximated a multipole with a slab of thickness

L equal to four times the distance d between ψ_s and ψ_c . The radiation cooling time was found from Eq. (50) to be

$$\tau_s = 2.5 \times 10^4 \left(\frac{R^2 n_{14}}{d(1-r)T_{\text{keV}}^3 B^3} \right)^{1/2} \text{ sec.} \quad (52)$$

For $B = 5$ T, $R = 4$ m, $n_{14} = 1$ (or $n = 10^{14} \text{ cm}^{-3}$), $T_e = 150$ keV, and $r = 99\%$, the value of $n\tau_s$ is $1.36 \times 10^{15} \text{ sec/cm}^3$, which is dangerously low for advanced fuels.

It should be noted that synchrotron radiation, like bremsstrahlung, is not an energy loss; radiation constitutes the entire fusion output of a neutronless reactor. Nonetheless, ignition will depend on how low synchrotron radiation can be made. Highly reflective walls for infrared radiation will be needed. The rippled nature of multipoles is expected to give some improvement, since the radiation from the interior is at low frequency and will be strongly reabsorbed in the bridge region. A calculation taking these complex geometrical factors into account is being performed⁸. Another beneficial effect³¹ is that high energy electrons and those in the bridge near the walls will preferentially be cooled by radiation, so that the losses will not be as bad as for a Maxwellian distribution.

MAGNETIC SHIELDING OF SUPPORTS

Most experiments to date with $N > 1$ have supported internal rings; the normal-conducting UW octupole is fully levitated, but the finite levitation time has caused difficulties in the interpretation of results. A reactor would surely require levitated superconductors. In that case, no large current feeds would be required, and it appears possible to design rings that float in stable mechanical equilibrium. Nonetheless, engineering design would be greatly facilitated by leads which carry liquid He coolant through the plasma. If these leads carry no current, they would suffer a heat load from particle bombardment as well as from photons and neutrons. Furthermore, plasma would be lost on the leads, causing a depletion of density on some lines of force and also the ejection of impurities. An asymmetry in electric potential would ensue, leading to enhanced convective losses. For these reasons, it is important to study the possibility of magnetic shielding of the leads by a running current along them. Massive neutron shielding would not be required if the leads are normal conductors.

The magnetic perturbation of a current dipole normal to a floating ring is shown in Fig. 11. It is seen that two magnetic

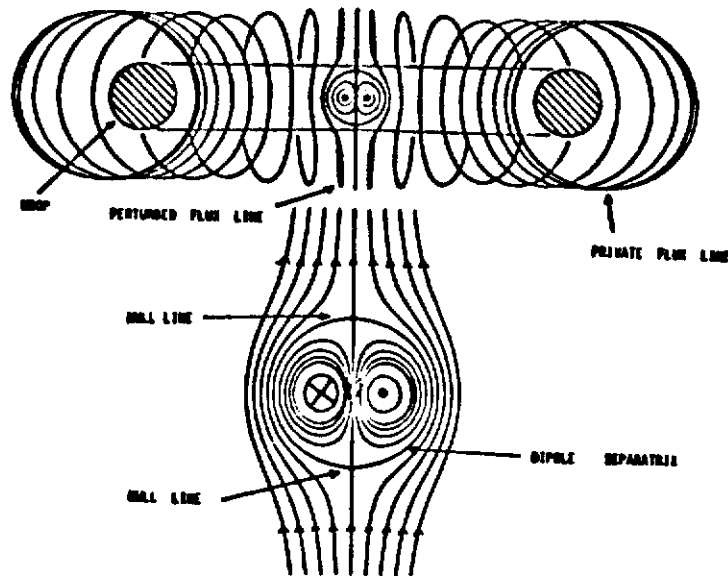


Fig. 11. Geometry of magnetically shielded supports
(From Ref. 30).

null lines are introduced which follow along the leads. Particles can escape along these nulls without being confined magnetically. Furthermore the introduction of an orthogonal field destroys the axisymmetry of the magnetic surfaces and can cause them to intersect the wall. Initial experiments³³ showed that magnetic guarding indeed reduced the particle flux to the supports but that the overall confinement was not greatly improved. Lehnert³⁴ pointed out that these early experiments did not disprove the ultimate usefulness of magnetic shielding. Three-dimensional effects, such as the reversal of the ∇B -drift of a particle as it passes the perturbed region, would greatly cancel the perturbation. These effects have been treated in detail by Lehnert³⁵, and we do not presume to summarize them here.

Recent data by Schumacher³⁶ have thrown light on the loss mechanism. The experiment was on the UCLA dodecapole (Fig. 4) with bridge field $B = 2.3$ kG, and two support wires 8 mm in diam and 14 mm apart, carrying 50 kA. Photographs of the plasma near the supports, looking upwards in Fig. 11, showed three streaks of light: along the side of the support, where the plasma flowed around them and was seen tangentially, and between wires, where the plasma flowed along the null lines. Particle collectors between the supports measured the current of ions lost by the ∇B -drift in the direction of the wires. This drift changes sign

across the support midplane, giving rise to a potential gradient between wires. The resulting $E \times B$ drift, always in the outward direction, has a magnitude intermediate to the ion and electron $B \times \nabla B$ drifts, as if an ambipolar mechanism were operative. The loss region has width $\approx 2 \rho_1$. This loss mechanism was predicted and has now been seen. The support loss was computed to be 60 times lower than for unguarded wires. Clearly, experiments with longer confinement times are needed to clarify the situation with magnetic shielding.

SUMMARY

The feasibility of multipole-surmac advanced-fuel reactors depends on three critical physics questions. Of these an accurate theoretical calculation of synchrotron radiation losses seems the most urgent. The second question is that of the β limit. Here one requires incorporation of finite Larmor radius into the theory. Present experiments are limited by the small number of gyroradii in the bridge region, and by collisions, particularly charge exchange. It appears that larger, more expensive devices will be needed to test predictions on the β limit. The third question is that of transport loss rate. Experience to date indicates that diffusion of collisionless plasmas will be dominated by convection in thermally generated vortices. A small toroidal field may be needed to lower these losses. The effect of trapped-particle microinstabilities in the presence of a toroidal field has been insufficiently studied. In reactors there will be the additional effect of non-Maxwellian distributions. Again, a larger experimental device is needed for further progress.

To reduce the collisionality of present experiments, various heating methods, such as ICRH, ECRH, and neutral-beam injection have been tried. We have omitted this body of work because it is probably irrelevant to reactor-grade devices. The possibility of direct ion beam injection is one of the major advantages of multipoles and appears to be the easiest and most efficient way to heat a reactor.

ACKNOWLEDGMENTS

We are indebted to T. Samec for casting linear multipole theory into a simple form suitable for this review. We also thank R. W. Schumacher, S. Prager, and E. A. Adler for their latest results, and N. Amherd for lending an advance copy of Ref. 9.

REFERENCES

1. A. Y. Wong, Y. Nakamura, B. H. Quon, and J. M. Dawson, Phys. Rev. Letters 35:1156 (1975).

2. T. K. Samec, Y. C. Lee, and B. D. Fried, Phys. Rev. Letters 35:1763 (1975).
3. D. L. Mamas, R. W. Schumacher, A. Y. Wong, and R. A. Breun, Phys. Rev. Letters 41:29 (1978).
4. R. W. Schumacher, M. Fukao, A. Y. Wong, and K. Yatsu, Stable confinement of high beta collisionless toroidal plasma, UCLA PPG-459 (1980), submitted to Phys. Rev. Letters.
5. J. R. Ferron, G. Dimonte, A. Y. Wong, P. Young, and B. Leikind, MHD stability of an axisymmetric large diameter magnetic mirror, UCLA preprint PPG-541 (1981).
6. T. Ohkawa and D. W. Kerst, Nuovo Cimento 22:784 (1961).
7. D. A. D'Ippolito, E. A. Adler, and Y. C. Lee, Phys. Fluids 23:794 (1980).
8. T. Samec, Ref. 9 and private communication.
9. TRW Group, EPRI Project Report RP-1190, Electric Power Research Institute, Palo Alto, California (to be published, 1981).
10. I. B. Bernstein, E. A. Frieman, M. D. Kruskal, and R. M. Kulsrud, Proc. Roy. Soc. London A244:17 (1958).
11. J. L. Johnson, R. M. Kulsrud, and K. E. Weimer, Plasma Phys. 11:463 (1969).
12. E. A. Adler and Y. C. Lee, Phys. Fluids 23:228 (1980).
13. S. C. Prager, J. H. Halle, M. W. Phillips, R. S. Post, and J. C. Twichell, Nuclear Fusion 20:635 (1980).
14. J. H. Halle, A. G. Kellman, R. S. Post, S. C. Prager, E. J. Strait, and M. C. Zarnstorff, Observations of High β Toroidal Plasmas, Wisconsin preprint, submitted to Phys. Rev. Letters (1981).
15. E. A. Adler and Y. C. Lee, Stability of Multipoles to Ballooning Modes with Large Toroidal Mode Number, UCLA PPG-507 (1980); Phys. Fluids, to be published.
16. G. A. Navratil and R. S. Post, An Interpretation of Multipole Confinement Experiments, Comments on Plasma Physics and Controlled Fusion 5, No. 2:29 (1979).
17. T. Ohkawa, J. R. Gilleland, T. Tamano, T. Takeda, and D. K. Bhadra, Phys. Rev. Letters 27:1179 (1971).
18. T. Ohkawa, M. Yoshikawa, R. E. Kribel, A. A. Schupp, and T. H. Jensen, Phys. Rev. Letters 24:95 (1970).
19. T. Tamano, R. Prater, and T. Ohkawa, Phys. Rev. Letters 30:431 (1973).
20. H. Okuda and J. M. Dawson, Phys. Fluids 16:408 (1973).
21. A. J. Cavallo, Phys. Fluids 19:394 (1976).
22. J. R. Drake, J. R. Greenwood, G. A. Navratil, and R. S. Post, Phys. Fluids 20:148 (1977); A. B. Ehrhardt, and R. S. Post, Measurement of Convective Cell Spectra and the Resultant Calculated Vortex Diffusion Coefficient, Wisconsin preprint DOE/ET53051/12 (1980).
23. G. A. Navratil and R. S. Post, Phys. Fluids 20:1205 (1977).

24. G. A. Navratil, R. S. Post, and A. B. Ehrhardt, Phys. Fluids 20:156 (1977) and 22:241 (1979).
25. A. B. Ehrhardt, H. R. Garner, G. A. Navratil, and R. S. Post, Cross Field Diffusion and Fluctuation Spectra in a Levitated Octupole in the Presence of a Toroidal Field, Wisconsin preprint DOE/ET53051/14 (1980).
26. T. Ohkawa, J. R. Gilleland, and T. Tamano, Phys. Rev. Letters 28:1107 (1972).
27. D. E. Lencioni, J. W. Poukey, J. A. Schmidt, J. C. Sprott, and C. W. Erickson, Phys. Fluids 11:1115 (1968).
28. T. Tamano, Y. Hamada, C. Moeller, T. Ohkawa, and R. Prater, Plasma Physics and Controlled Nuclear Fusion Research 1974, II:97, IAEA, Vienna (1975).
29. J. R. Drake, D. W. Kerst, G. A. Navratil, R. S. Post, E. Ejima, R. LaHaye, C. P. Moeller, T. Ohkawa, P. I. Peterson, R. Prater, and S. K. Wong, Plasma Physics and Controlled Nuclear Fusion Research 1976, II:333, IAEA, Vienna (1977).
30. R. W. Schumacher, Thesis, UCLA (1979).
31. J. M. Dawson, Alternate Concepts on Controlled Fusion, Part C: Fusion Reactor Using the $p\text{-}^{11}\text{B}$ Reaction, EPRI Report ER-429-SR, Electric Power Research Institute, Palo Alto, California (1977).
32. B. A. Trubnikov, in: "Reviews of Plasma Physics," M. A. Leontovich, ed., Consultants Bureau, New York, Vol. 7, p. 345 (1979).
33. For instance, A. W. Molvik, Phys. Fluids 15:1128 (1972).
34. B. Lehnert, Phys. Fluids 12:2710 (1969).
35. B. Lehnert, Plasma Physics 17:501 (1975).
36. R. W. Schumacher, private communication.

MULTIPOLES AND SURMACS II: ENGINEERING

Francis F. Chen

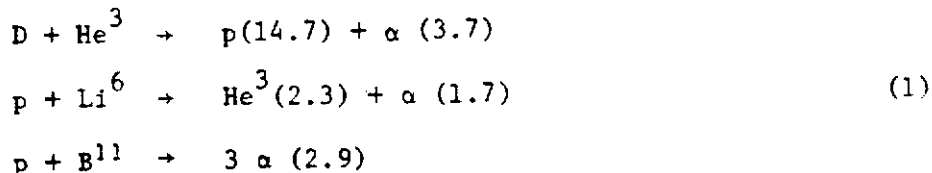
Electrical Sciences and Engineering Department
University of California
Los Angeles, California 90024

INTRODUCTION

Though the engineering of multipoles is in many ways simpler than for toruses with strong toroidal and poloidal fields, the feasibility of multiple floating rings in a reactor environment is of great concern, since it has never been demonstrated even in theory. Recent work by the group at TRW, Inc. and the groups led by R. W. Conn at Wisconsin and UCLA has greatly expanded our data base on the engineering aspects of multipoles. These studies are by no means commensurate with the studies of the physics problems, which have a long history. Nonetheless, there is much more known than can be covered here. The brevity of Part II is due partly to the nature of the calculational results, which are hard to condense, and partly to the necessity to design for specific devices, a process whose results may not be of general or timeless value. A summary of these results already exists¹.

ADVANCED FUEL CYCLES

To evaluate fusion fuel cycles from D-D to p-B¹¹, accurate measurements of many cross sections are needed. The most complete compilation to date was made by a panel of experts assembled by TRW, Inc. and EPRI². For multipole-surmacs these primary reactions producing few neutrons are of greatest interest:



The particle energies are indicated in MeV. Latest cross sections are shown in Fig. 1. Initial optimism on the p-Li⁶ reaction was based on a possible chain reaction involving the energetic He³ product³. However, the reaction He³ + Li⁶ → D + Be⁷ leads to many subsequent events producing neutrons, and a detailed investigation of p-Li⁶ would involve a very complex calculation requiring cross sections that are not well known. Current interest has centered on the "lean" D-He³ reaction, suitable for a low-neutron satellite reactor, and the p-B¹¹ reaction, which has been revived by the calculations of Shuy and Conn⁴.

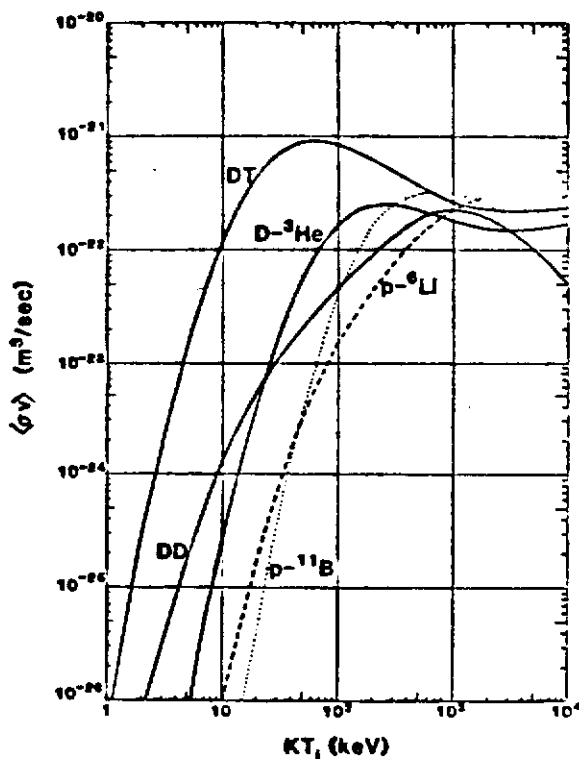


Fig. 1. Advanced fuel reactivities compared to DT.

These authors have calculated the improvement in reactivity due to the interaction of reaction products with the thermal fuel for the D-D, D-He³, and p-B¹¹ cycles. There are four physical processes that are usually neglected when the ash particles are considered to be gradually slowed down by small-angle collisions with the thermal distributions of electrons and fuel ions.

1) Nuclear elastic and inelastic scattering becomes important

relative to Coulomb interactions at typical ash energies of 10 MeV and typical fuel temperatures of 100 keV. Knock-on events produce a high energy tail in the fuel distribution which greatly enhances the probability of fusion. 2) Large-angle Coulomb collisions also populate the ion tail. 3) Thermalization of the tail particles among themselves helps by bringing the superfast particles down to energies near the peak of the fusion cross section. 4) Propagation of high-probability fusion reactions occurs as the processes above keep a high-energy tail populated. An example of a reaction propagation sequence is



where the bar indicates a hyperthermal particle. These do not have to be very abundant to affect the fusion rate because of the steepness of the curves in Fig. 1.

In the computations of Shuy^{4,5}, the ion distribution is divided into a Maxwellian body plus a tail. The body is treated as a continuum, subject to small-angle collisions isolated by adjusting the cutoff parameter in the Coulomb logarithm Λ and to Coulomb-nuclear interference treated by a weighting factor. The tail is subjected to the high energy transfer events by a multi-group technique. Bremsstrahlung and ash removal are considered the only energy sinks. Since $T_e \geq 100$ keV is normal here, bremsstrahlung and electron-ion thermalization are treated relativistically.

The results are extremely encouraging. Fig. 2 shows the reactivity enhancement⁴ due to processes (1)-(4) for the p-B¹¹ reaction, whose main branch is a decay into an α and a Be⁸ nucleus in an excited state, which subsequently decays into two α 's. The enhancement is sensitive to T_e because of the Coulomb drag. When these data are used to compute Q , the values in Table I, showing the possibility of ignition, are obtained^{4,1}. Here Q is the ratio of fusion power to heating power, M the ratio of fusion power to bremsstrahlung and ash removal loss power, and $n\tau_E$ is evaluated for $Q = 5$. The requirements on $n\tau_E$ are about an order of magnitude higher than for DT; furthermore the necessity for large T_e raises problems with synchrotron radiation (see Part I), which has been neglected here. Nonetheless, the results on ion tail promotion encourages further pursuit of the p-B¹¹ cycle, which is almost neutron free. The endothermic reaction $p + B^{11} \rightarrow n + C^{11}$ has a branching ratio $\approx 10^{-3}$.

Similar calculations⁴ for the D-He³ cycle yield the Lawson

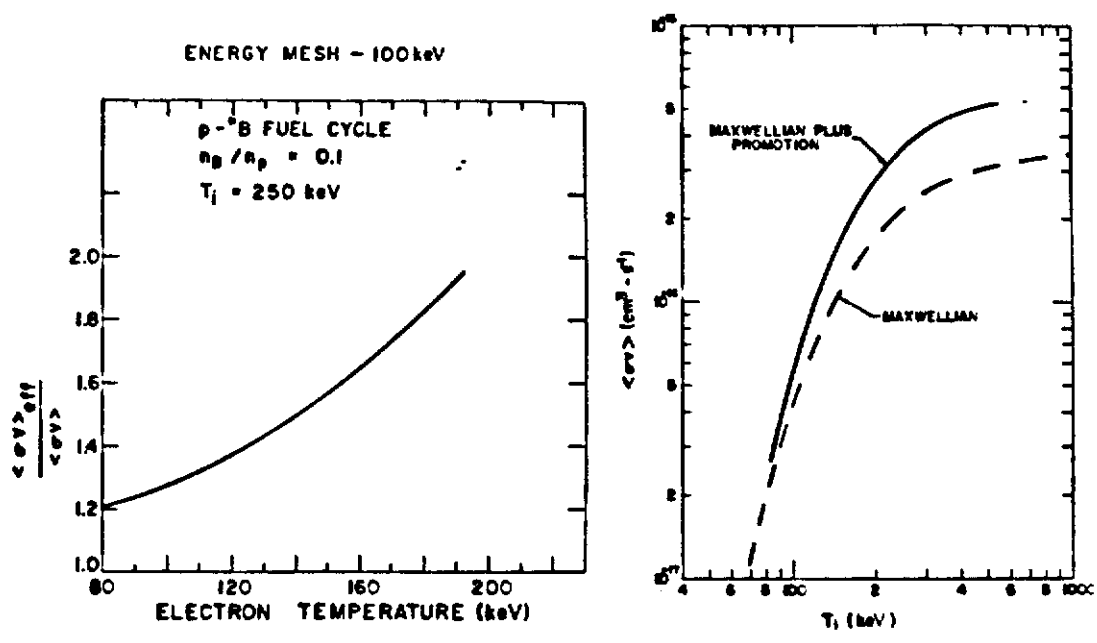


Fig. 2. Reactivity enhancement factor vs. T_e at $T_i = 250 \text{ keV}$, and reactivity vs. T_i at $T_e = 160 \text{ keV}$.

Table I. Requirements for a p-B¹¹ Reactor⁴.

| T_i (keV) | T_e (keV) | M | Q | $n\tau_E$ (sec/cm ³) |
|-------------|-------------|------|----------|----------------------------------|
| 200 | 140 | 0.8 | 4 | -- |
| 250 | 155 | 0.97 | 32 | 2.4×10^{15} |
| 300 | 160 | 1.08 | ∞ | 1.36×10^{15} |

curves shown in Fig. 3a. Here the effects of tail promotion lowers the ignition $n\tau_E$ to $3 \times 10^{14} \text{ sec/cm}^3$ at $T_i = 100 \text{ keV}$, the same as for DT at 20 keV. For multipoles, there is then the problem of shielding against the neutrons. Fig. 3b shows the effect on neutron heat load and fusion power of increasing the density ratio of He³ to D. Neutron production can be greatly reduced, but only at the expense of fusion power. For ratios greater than 8, ignition cannot be achieved with D-He³.

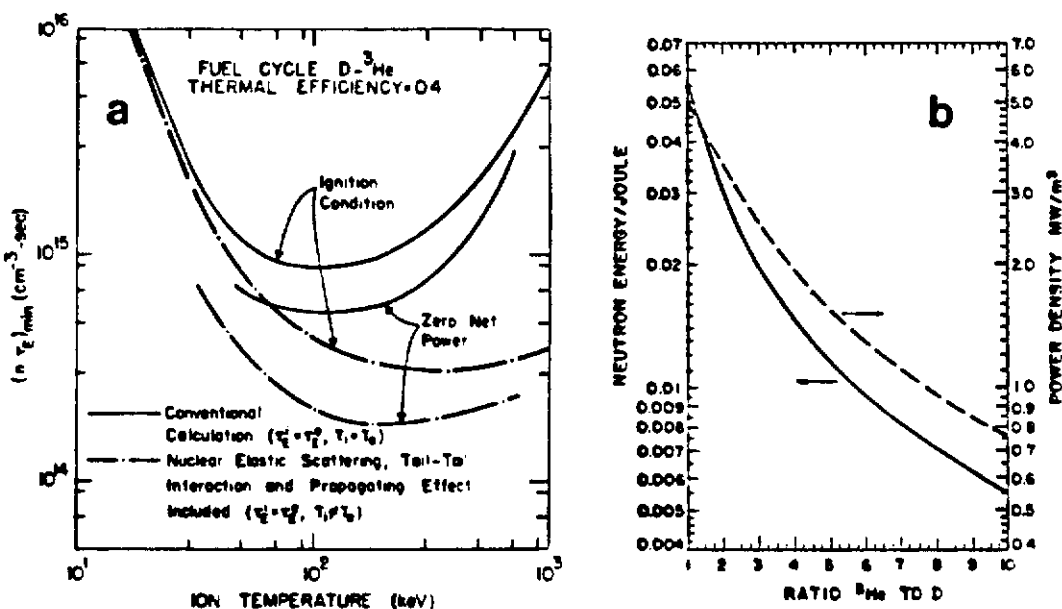


Fig. 3. (a) Improvement of Lawson condition for D-He³ with ion tail formation. (b) Effect on neutron energy and fusion power of running a lean mixture of D and He³.

DESIGN OF SUPERCONDUCTING RINGS

The most critical elements in the design of a multipole or surmac reactor are the superconducting levitated rings, which must maintain an internal temperature of $\leq 10^\circ \text{K}$ while immersed in a reacting plasma of $\geq 2 \times 10^9^\circ \text{K}$. The superconductor must be well shielded; the minor diameter of the rings will therefore be of order 1 m or larger. This consideration sets the scale of the entire reactor. There are at least three ways in which the superconductor can be cooled. First, if magnetically shielded leads are possible, one can imagine continuous circulation of liquid He from the outside. Second, since the rings receive more radiation from the side facing the plasma than the side facing the wall, a temperature gradient will develop across the minor diameter; and one can conceive of incorporating a refrigeration system within each ring that will be driven by this temperature difference. The exhaust heat of the internal cryostat will be radiated away from a high-temperature surface to the outside wall. Third, one can simply replace the rings after their warm-up time of a few days with another set that has been cooled in an adjacent chamber. This conservative approach is the one taken in the three designs described here. The feasibility of levitating a single superconducting ring has already been demonstrated in numerous levitron and spherator experiments.

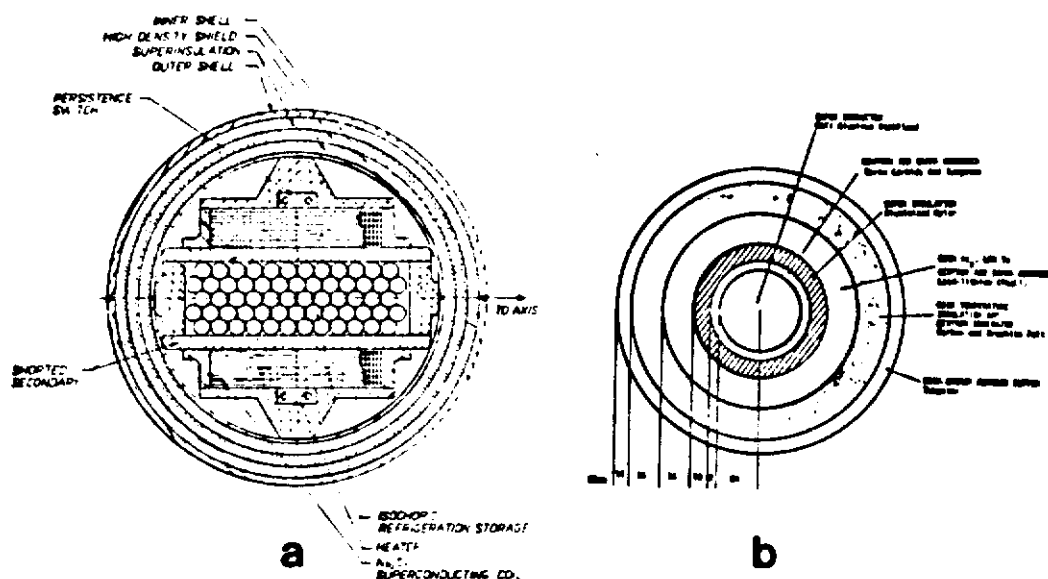


Fig. 4. Superconducting ring designs for (a) a proof-of-principle experiment, and (b) a conceptual D-He³ reactor. (Ref. 2)

The first design, shown in Fig. 4a, is for a proof-of-principle experiment². This ring can remain superconducting for an experimental time of about five hours. Partly to test new technology, it is designed not with NbTi but with multifilament Nb₃Sn wire, which has a critical current density ten times less sensitive to temperature changes at 4.5°K than NbTi. The 4- μ m diam filaments are imbedded in a 2 \times 1 mm matrix, 2200 turns of which carry 909 A each, for a total of 2 MA, 3 to 6 times larger than presently achieved. Protection of the superconductor is by good thermal and electrical contact to thick Al plates, cooled by a reservoir of He providing 1.2×10^4 J of heat capacity between 4.2 and 6.5°K. Peak field is 6.4 T, and stored magnetic energy is 9.6 MJ in the 2 m major by 15.5 cm minor diam coil.

The second design² (Fig. 4b) is a much larger ring shielded against the neutron and x-ray flux of a conceptual D-He³ reactor. The outside layer is 14 cm of tungsten, which serves both to radiate absorbed x-ray and particle energies at 2000°K and to moderate the neutron spectrum. A layer of high temperature carbon insulation further softens the spectrum. Gamma rays generated in the outer layers are absorbed in a Pb₄Li layer which melts at 507°K and provides thermal capacity. Aluminized mylar superinsulation follows, and a B₄C and W gamma absorber is added inside the superinsulation. The superconductor is NbTi stabilized with Al in a Cu matrix. Construction of the superconductor and dewar is shown in Fig. 5. The coil carries 4.8 kA/cm² at 8 T. The fractional volumes

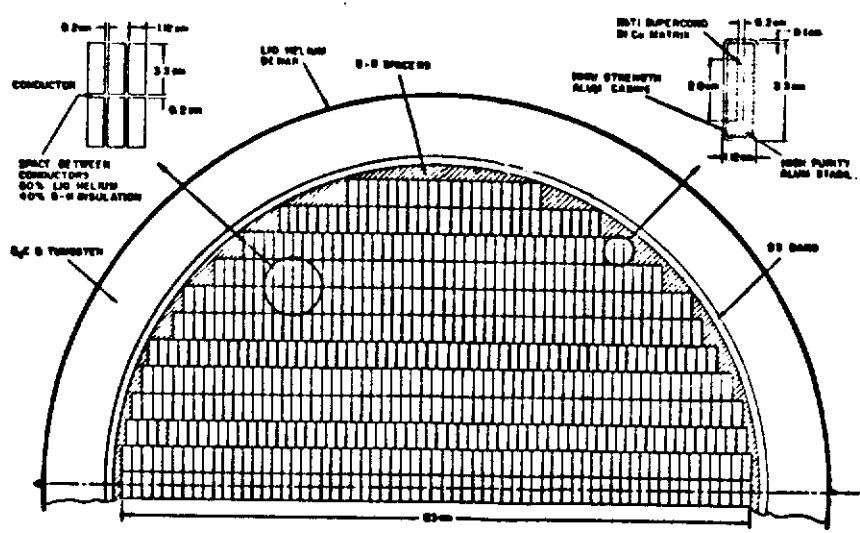


Fig. 5. Superconductor design for conceptual multipole reactor. (Ref. 2)

in the conductor region are: superconductor (18%), Al stabilizer (48%), copper (9%), and liquid He (15%).

Heating of the ring was computed as if it were ≈ 6 m away from a 4.6 m-diam reacting D-He³ plasma. Fig. 6 shows the neutron energy spectrum in such a case; it is dominated by 2.5-MeV D-D and 14-MeV D-T neutrons. The temperature rise in the various layers was then computed under quasi-steady state heating, mainly by the capture of neutrons and of the gamma rays generated thereby. Fig. 7a shows the reduction in neutron flux by the shielding, and Fig. 7b shows the associated volumetric heat source distribution. The ring construction reduces the neutron flux on the axis to $6.3 \times 10^8 \text{ cm}^{-2} \text{ sec}^{-1}$ and the neutron and gamma energy fluxes to 2.5×10^8 and $1.8 \times 10^8 \text{ MeV/cm}^2 \text{ sec}$, respectively. The temperature in the superconductor rises at 0.2°K/hr , allowing operation for the order of a day in this non-optimized design. Neutron damage was also assessed; less than 1% change in resistivity was expected after one year.

The most recent study⁶ of a floating ring design is shown in Fig. 8. The ring is used to provide min-B stability in an axisymmetric tandem mirror. The structure of the shielding and insulation is given in Fig. 9. A thermal flux of 45 W/cm^2 is assumed to be incident on the tungsten outer surface in the one dimensional calculation. In addition, the volumetric heating due to neutrons from a D-He³ burn in the geometry of Fig. 8 was included. It is seen from Fig. 9 that the neutron shield in this design holds the temperature of the superconductor below 8°K for the order of five days. With surface heating alone, the time would have been

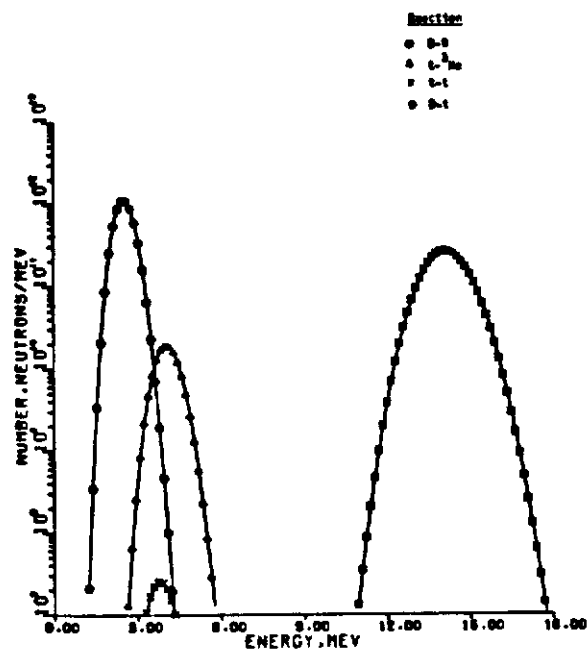


Fig. 6. Neutron energy distribution in a D-He³ reactor. (Ref. 2)

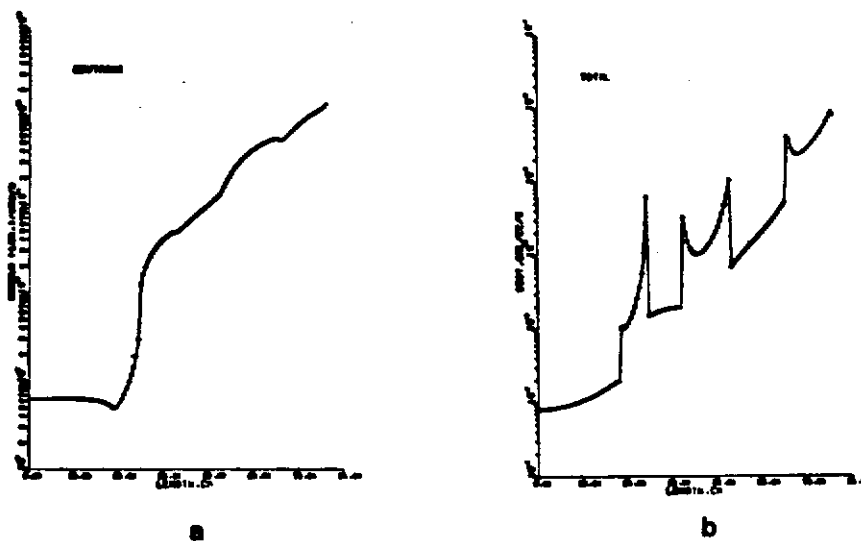


Fig. 7. Neutron flux (a) and volumetric heat source (b) distribution in the ring of Fig. 4. (Ref. 2)

extended to the order of one month. From these computations, it appears that floating rings can be designed for sufficiently long cold times even in the neutron environment of a D-He³ reactor.

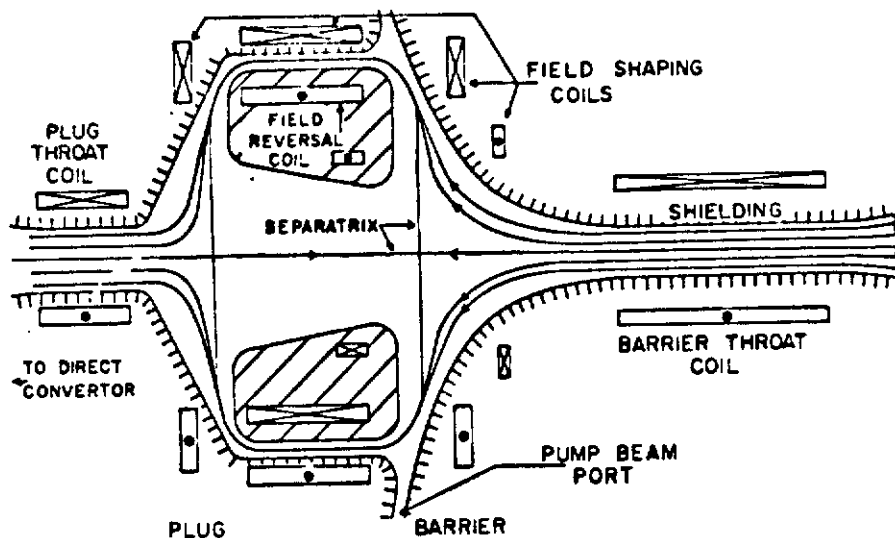


Fig. 8. Geometry of a floating coil designed for an axisymmetric mirror (Ref. 6).

REACTOR DESIGN

We summarize here the main features of a conceptual D-He³ reactor designed by the TRW group². The size and layout of the octupole are shown in Fig. 10, and the numerical parameters in Table II.

In designing the ring sizes, positions, and currents, a compromise has to be made between the engineering constraint of low hoop force and the physics requirement of good well depth. Furthermore, one has the option of adding an overall bias field to equalize the fields at the bridges of the inner and outer hoops, which tend to differ by about a factor of two. Such a bias field would make better use of the B_{crit} of superconductors and at the same time decrease the mirror ratio and thus tend to suppress trapped-particle instabilities. The present design has a tensile stress on the inner ring and a compressive stress on the outer ring. The upper and lower rings are separated by externally cooled wall hoops carrying about 10 MA. The design is by no means optimized, but it does show that ring stresses and weights can be achieved which are not excessive. The large stored energy is, however, a cause of concern; if one hoop should go normal, some means must be devised to handle the enormous electrical and mechanical loads on a time scale of tens of seconds.

Since most of the fusion power output from an advanced-fuel reactor is in the form of bremsstrahlung x-rays, the heat load on the rings and on the first wall must be considered carefully. The

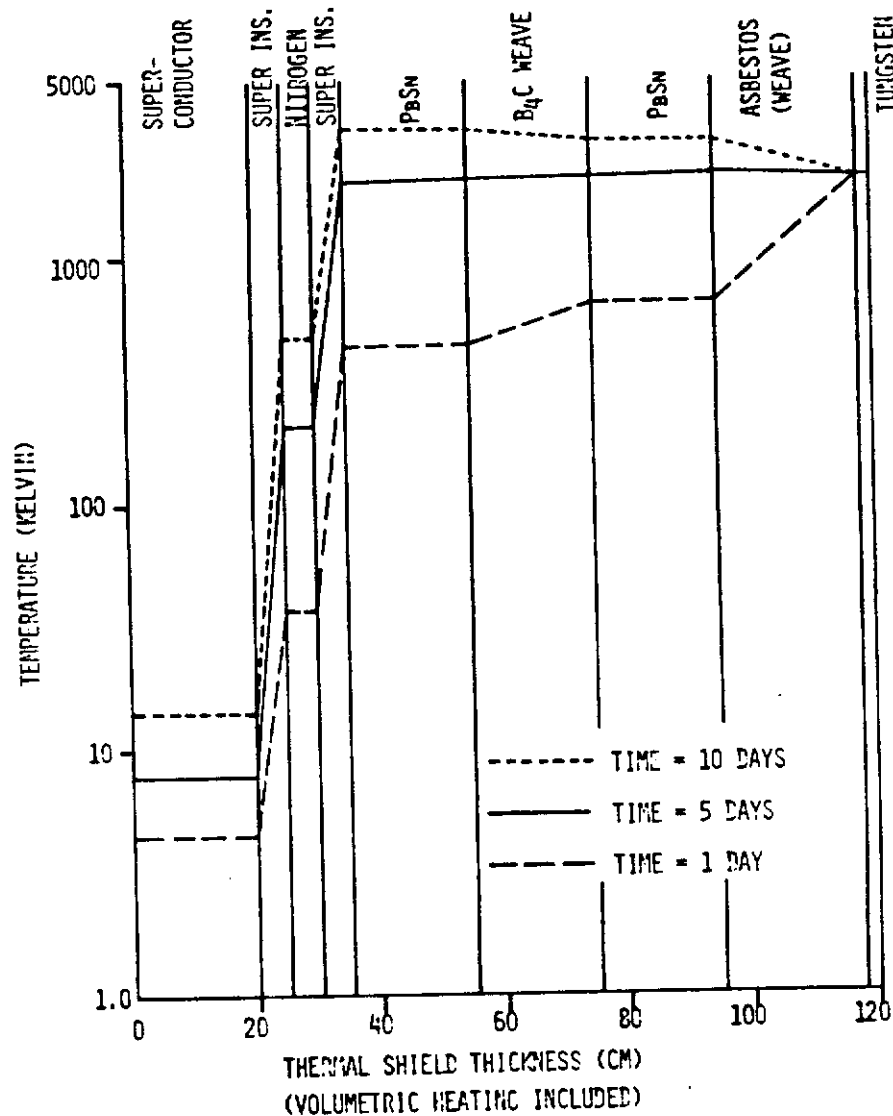


Fig. 9. Temperature distribution in coil of Fig. 8 with volumetric neutron heating (Ref. 6).

floating rings are cooled by radiation from the tungsten surface, limited to a rate of $\approx 1 \text{ MW/m}^2$ at 2000°C . The design of Fig. 10 yields a maximum x-ray flux of 0.69 MW/m^2 on the rings; a further margin of safety can be obtained if the heat is redistributed over the surface by heat pipes. The first wall receives $0.3\text{--}1.11 \text{ MW/m}^2$ x-ray flux, with an average of 0.46 MW/m^2 , well below the wall loading of DT reactor designs. However, the heat load is not well distributed over the volume of the wall. For instance, at $KT_e = 150 \text{ keV}$, 70% of the heat is deposited in the first 0.2 mm of an

80% Va - 20% Ti first wall. The wall material will have to be optimized in regard to mechanical and thermal properties, low-Z contamination, toxicity, and reflectivity for synchrotron radiation; this has not yet been done.

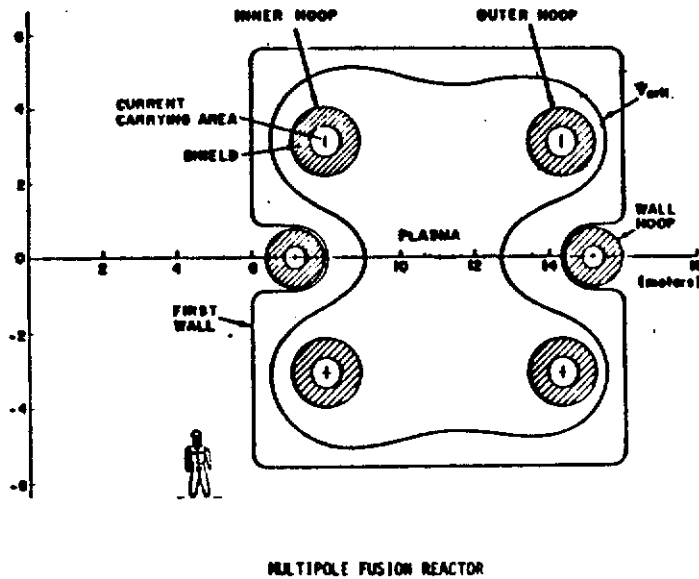


Fig. 10. Schematic of a conceptual D-He³ octupole reactor (Ref. 2).

Table II. Parameters for Conceptual D-He³ Octupole Reactor

| | | | |
|-------------------------------|---------------------|---------------------|------------------------|
| Major radius | 10.8 m | Ring current (each) | 17 MA |
| Plasma volume | 4120 m ³ | Power density | 0.34 W/cm ³ |
| B _{max} on conductor | 9.0 T | Power output | 1400 MW _{th} |
| B at ψ_c | 3.7 T | Gross elec. power | 600 MW _e |

| | <u>Inner rings</u> | <u>Outer rings</u> |
|-----------------------|--------------------|--------------------|
| Major radius (m) | 8.0 | 14.4 |
| Stored energy (GJ) | 5.3 | 11 |
| Force on ring (MN) | -18.6 | +28.0 (compr.) |
| Mass of ring (tonnes) | 1200 | 2160 |

This reactor design also included two possible power cycles, a steam cycle at 540°C and a helium gas-turbine Brayton cycle at 870°C, both providing $\approx 44\%$ efficiency with present technology. The problems of impurity control, refueling, and ash removal remain to be solved, as with mainline approaches. However, ash removal is a particularly critical problem in advanced-fuel reactors because the fraction of available β used to confine the reaction products decreases the already low value of fuel density.

RING STABILITY

The critical problem of mechanically stabilizing the floating rings has been examined by several independent workers, and the situation is summarized in Ref. 2. Since the rings carry current in the same direction, they attract one another and must be separated by large forces provided by currents in the walls or external coils. Each ring has five degrees of freedom: slide in two directions, tilt around two axes, and vertical displacement. Stability of pulsed multi-ring systems has been demonstrated by the Wisconsin octupole and the UCLA dodecapole. The long-term stability of superconducting rings, however, has been achieved only with active feedback and only on single-ring systems. Reliance on passive stabilization alone would obviously be desirable in a reactor. A study by the TRW group² shows that the use of shorted turns in the shape shown in Fig. 11 would stabilize one motion at a time. The simultaneous stabilization of many rings interacting with one another using passive conductors well outside the plasma has not yet been shown possible, but it is believed that at worst only a small amount of active feedback control needs to be added to a passive system. L. Heflinger⁷ has invented a clever device to test stabilizing windings. A small model is constructed, and the inductance of a given hoop is used as part of the resonant circuit of an oscillator. Motion of the hoop changes the frequency of the oscillator up or down depending on how the inductance is changed. The existence of a stable, maximum inductance state is then easily discovered.

OTHER STUDIES

A step-by-step program to investigate the ultimate feasibility of multipole reactors has been proposed². The elements are a) a large octupole, using cryogenic but not superconducting Al rings, for testing the physics scaling of confinement time and beta limits up to kilovolt temperatures, using neutral beam heating; b) a technology validation test of a large superconducting Nb₃Sn ring; c) a tabletop superconducting experiment to test

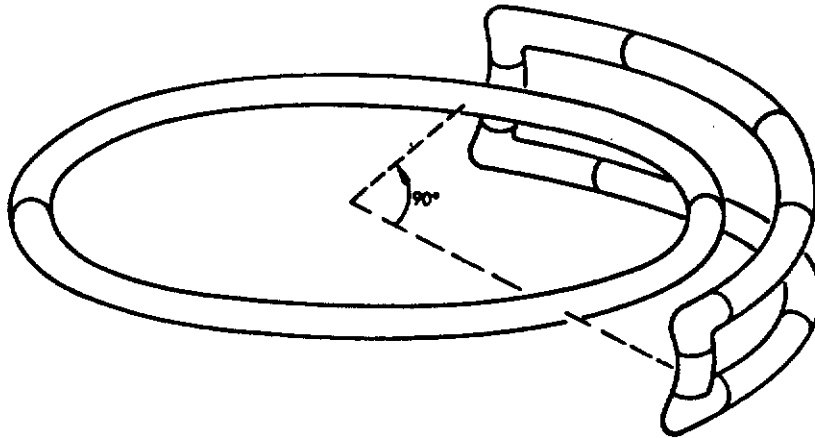


Fig. 11. A passive quadrant stabilizer for a floating ring.

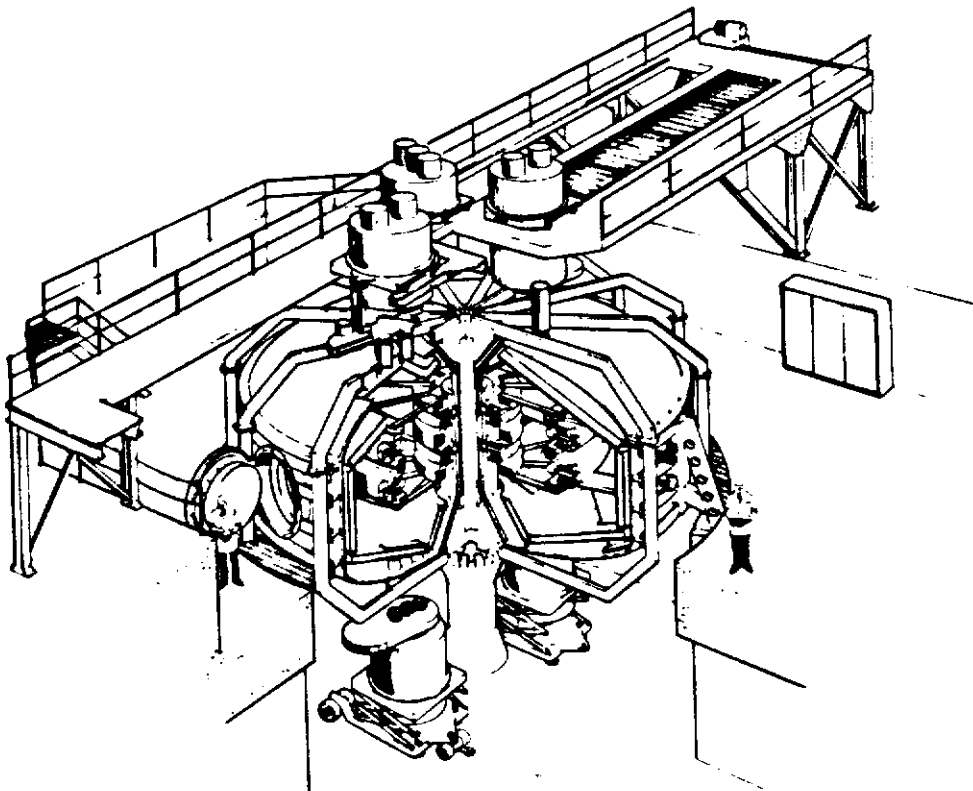


Fig. 12. A cryogenic octupole designed for test of scaling laws.

stabilization of octupole rings; and d) a large proof-of-principle experiment using these technological developments. The first of these devices has been designed in some detail; a sketch of it is shown in Fig. 12. Though multipole-surmac reactors are less well developed in concept than DT reactors in tokamak or tandem mirror configurations, it appears that an orderly progression of physics and engineering test devices is possible to examine the feasibility of the concept once the basic question of nuclear reaction rates is settled.

FUTURE POSSIBILITIES

The multipole-surmac advanced-fuel reactor concept provides an opportunity for generating new, daring ideas. One of these, the idea of building a liquid He cryostat into each floating ring, has already been mentioned. Another unconventional scheme, also not developed beyond the initial thought stage, has been proposed by A. Hertzberg⁸. Here, use is made of the fact that the x-ray output of a neutronless fuel cycle constitutes a high-grade form of energy. The x-rays pass through a thin, low-Z first wall (Fig. 13) and are absorbed by a high-Z gas coolant. Alternatively, tungsten glow-plates can be used to absorb the x-rays and heat the coolant gas by contact. A temperature gradient across the gas allows the outlet temperature to be higher than the wall temperature, thus increasing the thermal efficiency above the normal 40% level. The hot gas is then expanded in a rotating acoustic wave convertor (Fig. 14) to drive a high-pressure helium turbine. It is estimated that efficiencies of 50-65% may be possible.

A third idea, well within the realm of possibility, has been proposed by Dawson⁹ for heating plasmas by means of beams of partially ionized light ions. For instance, 100 A of 10-MeV Li^+ ions would give 1 GW of heating power. Though accelerators of this voltage-current range do not exist, they are not far beyond present capabilities. The light ions would be fully stripped by the plasma and become trapped. Good injection orbits for a tokamak are somewhat difficult to achieve, since it is best to inject from the inside of the torus, where there is little space; but injection into a multipole-surmac would be quite simple. Fig. 15a shows the dimensions of a conceptual p-B¹¹ dodecapole surmac reactor for which some numerical computations have been made¹⁰. Fig. 15b shows the path of an injected 10-MeV B¹¹ ion before it is ionized to Z=2. Figs. 15c and 15d show the paths of the ion while in the Z=3 and Z=4 states. It is seen that the ions are easily trapped and trace out the bridge regions clearly. Ions in this energy range are indistinguishable from the promoted tail of the distribution function and can be treated in the same manner. Plasma heating is probably not the most difficult problem in an advanced-fuel multipole.

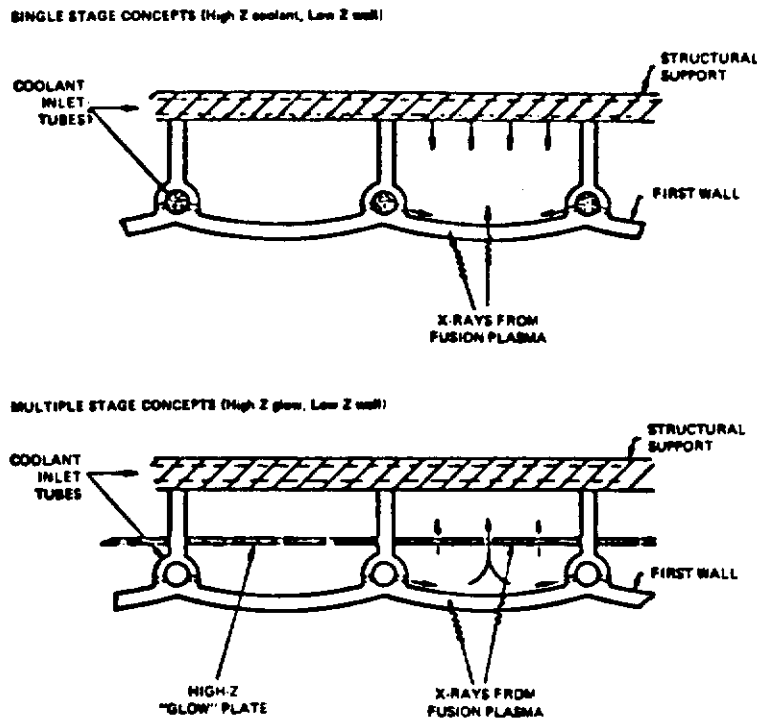


Fig. 13. First-wall design for absorption of x-ray energy output.

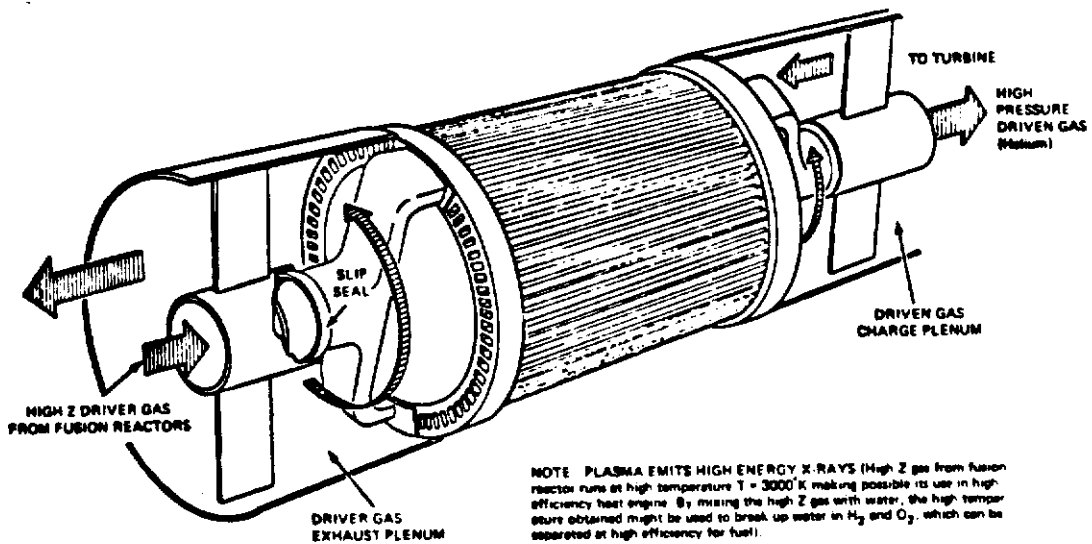


Fig. 14. High-efficiency heat engine employing high-Z driver gas.

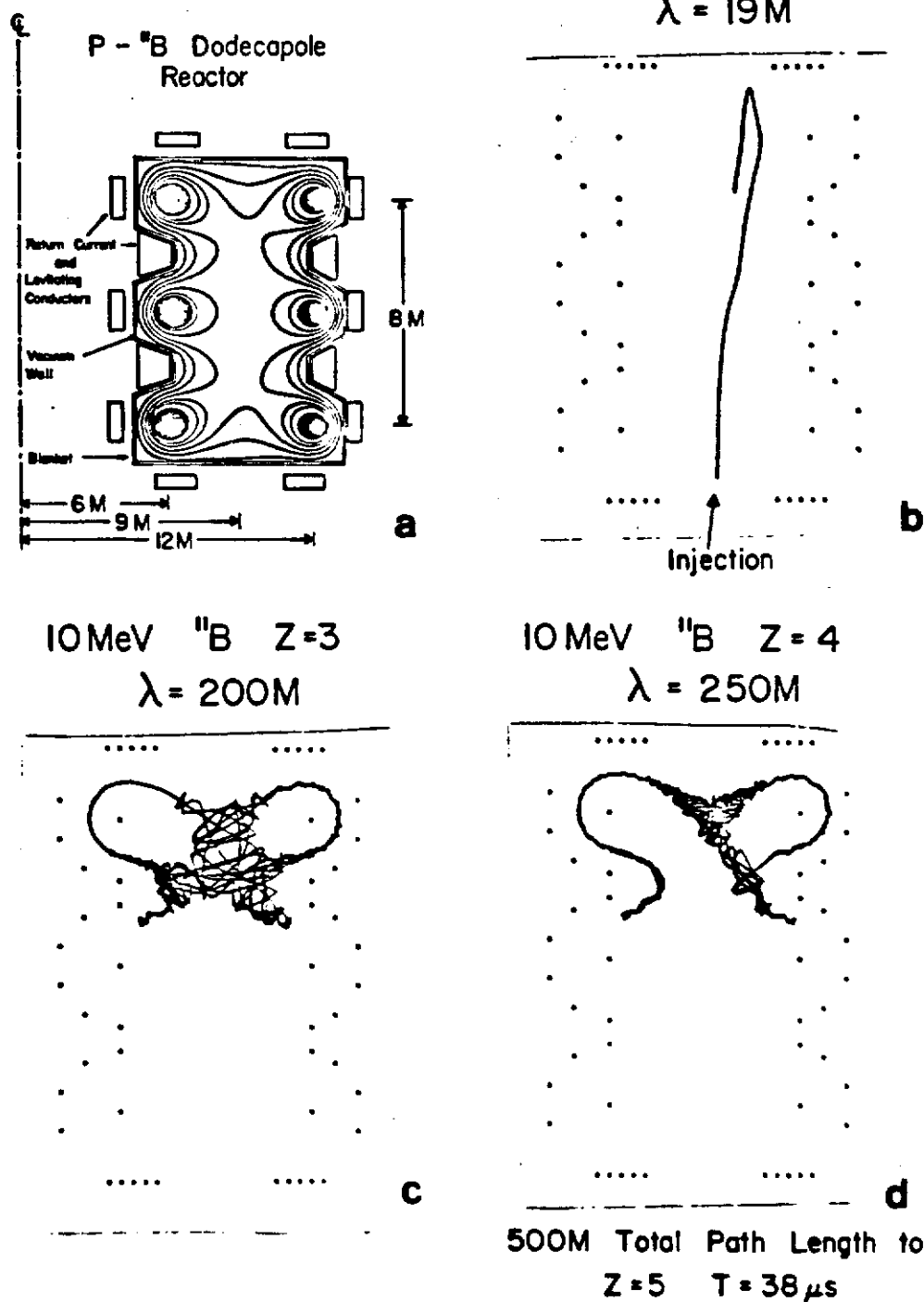


Fig. 15. Ion beam heating of a surmac reactor (a). The path of a 10-MeV B^+ injected ion is shown in (b)-(d) as it goes through the $Z=1$ to $Z=4$ ionization states.

ACKNOWLEDGMENTS

We have had the benefit of conversations with R. W. Conn, G. Shuy, S. Grosz, L. Heflinger, R. Schumacher, and J. M. Dawson. We are particularly grateful to R. W. Conn and his colleagues for releasing the results of their computations for this review in advance of their publication.

REFERENCES

1. R. W. Conn et al., Alternate fusion fuel cycle research, Plasma Physics and Controlled Nuclear Fusion Research 1980, paper IAEA-CN-38/V-5, IAEA, Vienna (1981, to be published).
2. TRW Group, EPRI Project Report RP-1190, Electric Power Research Institute, Palo Alto, California (1981, to be published).
3. R. W. Conn and G. Shuy, Univ. of Wisconsin Report UWFDM-262 (1978).
4. G. W. Shuy and R. W. Conn, Physics phenomena in the analysis of advanced fusion fuel cycles, UCLA Report PPG-522 (1980).
5. G. W. Shuy, Thesis, University of Wisconsin (1980).
6. S. Grosz, UCLA, private communication.
7. L. Heflinger, TRW, private communication and Ref. 2.
8. A. Hertzberg, in The EPRI Asilomar Papers, EPRI Special Report ER-378-SR, Electric Power Research Institute, Palo Alto, California (1977).
9. J. M. Dawson, private communication.
10. R. W. Schumacher and G. Hockney, private communication.